SERIAL NO. SSC-38

COPY NO. 166

PROGRESS REPORT

ON

A STUDY OF PLASTIC DEFORMATION AND FRACTURING BY STRAIN ENERGY DISTRIBUTION

BY

S. I. LIU and S. T. CARPENTER

SWARTHMORE COLLEGE

Under Bureau of Ships Contract Nobs-45521

Transmitted through

NATIONAL RESEARCH COUNCIL'S

COMMITTEE ON SHIP STEEL

Advisory to

SHIP STRUCTURE COMMITTEE

under

Bureau of Ships, Navy Department

Contract NObs-50148

Division of Engineering and Industrial Research

National Research Council

Washington D. C.

December 20, 1950

NATIONAL RESEARCH COUNCIL
2101 CONSTITUTION AVENUE, WASHINGTON 25, D. C.

COMMITTEE ON SHIP STEEL
OF THE
DIVISION OF ENGINEERING AND INDUSTRIAL RESEARCH

December 20, 1950

Chief, Bureau of Ships
Code 343
Navy Department
Washington 25, D. C.

Dear Sir:

Attached is Report Serial No. SSC-38 entitled "A Study of Plastic Deformation and Fracturing by Strain Energy Distribution." This report has been submitted by the contractor as a Progress Report of the work done on Research Project SR-98 under Contract NObs-45521 between the Bureau of Ships, Navy Department and Swarthmore College.

The report has been reviewed and acceptance recommended by representatives of the Committee on Ship Steel, Division of Engineering and Industrial Research, NRC, in accordance with the terms of the contract between the Bureau of Ships, Navy Department and the National Academy of Sciences.

Very truly yours,

Robert F. Mehl

RFM:mh

R. F. Mehl, Chairman
Committee on Ship Steel

PREFACE

The Navy Department through the Bureau of Ships is distributing this report for the SHIP STRUCTURE COMMITTEE to those agencies and individuals who were actively associated with the research work. This report represents results of part of the research program conducted under the Ship Structure Committee's directive to "investigate the design and methods of construction of welded steel merchant vessels."

The distribution of this report is as follows:

Copy No. 1 - Chief, Bureau of Ships, Navy Department
Copy No. 2 - Dr. Douglas Whitaker, National Research Council

Ship Structure Committee

Copy No. 3 - Rear Admiral K. K. Cowart, USCG - Chairman
Copy No. 4 - Rear Admiral Charles D. Wheelock, USN, Bureau of Ships
Copy No. 5 - Captain R. L. Hicks, USN, Maritime Administration
Copy No. 6 - Captain W. N. Mansfield, USNR, Military Sea Transportation Service
Copy No. 7 - Col. Werner W. Moore, USA, Transportation Corps Board, Liaison
Copy No. 8 - D. P. Brown, American Bureau of Shipping

Ship Structure Subcommittee

Copy No. 9 - Captain C. M. Tooke, USN, Bureau of Ships - Chairman
Copy No. 10 - Comdr. E. A. Grantham, USN, Military Sea Transportation Service
Copy No. 11 - Comdr. R. H. Lambert, USN, Bureau of Ships
Copy No. 12 - Comdr. James McIntosh, USCG, U. S. Coast Guard Headquarters
Copy No. 13 - Comdr. R. D. Schmidtman, USCG, U. S. Coast Guard Headquarters
Copy No. 14 - W. G. Frederick, Maritime Administration
Copy No. 15 - Hubert Kempel, Military Sea Transportation Service
Copy No. 16 - I. R. Kramer, Office of Naval Research
Copy No. 17 - Lewis C. Host, American Bureau of Shipping
Copy No. 18 - Mathew Letich, American Bureau of Shipping
Copy No. 19 - E. M. MacCutcheon, Jr., Bureau of Ships
Copy No. 20 - V. L. Russo, Maritime Administration
Copy No. 21 - Finn Jonassen, Liaison Representative, NRC
Copy No. 22 - E. H. Davidson, Liaison Representative, AISI
Copy No. 23 - W. P. Gerhart, Liaison Representative, AISI
Copy No. 24 - Wm. Spraragen, Liaison Representative, WRC

Committee on Ship Steel

Copy No. 25 - R. F. Mehl, Chairman
Copy No. 26 - C. H. Herty, Jr., Vice Chairman
Copy No. 27 - Wm. M. Baldwin, Jr.
Copy No. 28 - Chas. S. Barrett
Copy No. 29 - R. M. Brick
Copy No. 30 - S. L. Hoyt
Copy No. 16 - I. R. Kramer
Copy No. 31 - M. W. Lightner
Copy No. 32 - T. S. Washburn
Copy No. 21 - Finn Jonassen, Technical Director
Copy No. 33 - James E. McNutt, Technical Secretary

Members of Project Advisory Committees SR-98, SR-99, SR-100, SR-108, SR-109, SR-110 and SR-111 (not listed elsewhere)

Copy No. 34 - R. H. Aborn
Copy No. 35 - E. A. Anderson
Copy No. 36 - L. C. Bibber
Copy No. 37 - Morris Cohen
Copy No. 38 - W. C. Ellis
Copy No. 39 - M. Gensamer
Copy No. 40 - M. F. Hawkes
Copy No. 41 - W. F. Hess
Copy No. 42 - W. R. Hibbard, Jr.
Copy No. 43 - C. E. Jackson
Copy No. 44 - P. E. Kyle
Copy No. 45 - J. R. Low, Jr.
Copy No. 46 - H. W. Pierce
Copy No. 47 - W. A. Reich
Copy No. 48 - C. E. Sims
Copy No. 49 - R. D. Stout
Copy No. 50 - J. G. Thompson
Copy No. 51 - Bruce G. Johnston, Welding Research Council, Liaison
Copy No. 52 - W. H. Wooding, Philadelphia Naval Shipyard

Committee on Residual Stresses

Copy No. 53 - John T. Norton, Chairman
Copy No. 27 - Wm. M. Baldwin, Jr.
Copy No. 54 - Paul Ffield
Copy No. 55 - Levan Griffis
Copy No. 56 - K. Heindlhofer
Copy No. 57 - Daniel Rosenthal
Copy No. 21 - Finn Jonassen, Technical Director
Copy No. 33 - James E. McNutt, Technical Secretary

Navy Department

Copy No. 58 - Capt. H. A. Ingram, USN, Supervising Inspector of Naval Materials
Copy No. 59 - Comdr. R. S. Mandelkorn, USN, Armed Forces Special Weapons Project
Copy No. 60 - Comdr. F. G. Springer, USN, Bureau of Ships
Copy No. 61 - A. Amirikian, Bureau of Yards and Docks
Copy No. 62 - A. G. Bissell, Bureau of Ships
Copy No. 63 - J. M. Crowley, Office of Naval Research
Copy No. 64 - Charles Hoch, Military Sea Transportation Service
Copy No. 65 - J. W. Jenkins, Bureau of Ships
Copy No. 66 - Noah Kahn, New York Naval Shipyard
Copy No. 67 - N. E. Promisel, Bureau of Aeronautics
Copy No. 68 - John Vasta, Bureau of Ships
Copy No. 69 - J. E. Walker, Bureau of Ships
Copy No. 70 - Naval Research Laboratory
Copy No. 71 - Naval Research Laboratory, Mechanical Section
Copy No. 72 - Naval Research Laboratory, Metallurgical Section

Copies 73 and 74 - U. S. Naval Engineering Experiment Station
Copy No. 75 - Post Graduate School, U. S. Naval Academy
Copy No. 76 - New York Naval Shipyard, Material Laboratory
Copy No. 77 - Industrial Testing Laboratory, Philadelphia Naval Shipyard
Copy No. 78 - Philadelphia Naval Shipyard
Copy No. 79 - San Francisco Naval Shipyard
Copy No. 80 - David Taylor Model Basin, Attn: Library
Copies 81 and 82 - Publications Board, Navy Department via Bureau of Ships, Code 362
Copies 83 and 84 - Technical Library, Bureau of Ships, Code 364

U. S. Coast Guard

Copy No. 85 - Captain R. B. Lank, Jr., USCG
Copy No. 86 - Captain H. C. Moore, USCG
Copy No. 87 - Captain G. A. Tyler, USCG
Copy No. 88 - W. E. Magee, U. S. Coast Guard
Copy No. 89 - J. B. Robertson, Jr., U. S. Coast Guard
Copy No. 90 - Testing and Development Division
Copy No. 91 - U. S. Coast Guard Academy, New London

U. S. Maritime Administration

Copy No. 92 - Vice Adm. E. L. Cochrane, USN (Ret.)
Copy No. 93 - E. E. Martinsky

Representatives of American Iron and Steel Institute
Committee on Manufacturing Problems

Copy No. 94 - C. M. Parker, Secretary, General Technical Committee, American Iron and Steel Institute
Copy No. 36 - L. C. Bibber, Carnegie-Illinois Steel Corp.
Copy No. 26 - C. H. Herty, Jr., Bethlehem Steel Company
Copy No. 95 - E. C. Smith, Republic Steel Corp.

Welding Research Council

Copy No. 96 - C. A. Adams
Copy No. 97 - Harry Boardman
Copy No. 98 - LaMotte Grover
Copy No. 24 - Wm. Spraragen

Copy No. 99 - C. R. Soderberg, Chairman, Div. of Engineering & Ind. Research, NRC
Copy No. 25 - R. F. Mehl, Chairman, Committee on Ship Steel
Copy No. 21 - Finn Jonassen, Technical Director, Committee on Ship Steel
Copy No. 100 - S. I. Liu, Investigator, Research Project SR-98
Copy No. 101 - S. T. Carpenter, Investigator, Research Project SR-98 and SR-118
Copy No. 27 - Wm. M. Baldwin, Jr., Investigator, Research Project SR-99 and 111
Copy No. 102 - L. J. Ebert, Investigator, Research Project SR-99

Copy No. 103 - L. J. Klingler, Investigator, Research Project SR-99
Copy No. 104 - C. B. Voldrich, Investigator, Research Project SR-100
Copy No. 105 - P. J. Rieppel, Investigator, Research Project SR-100
Copy No. 106 - M. L. Williams, Investigator, Research Project SR-106
Copy No. 25 - R. F. Mehl, Investigator, Research Project SR-108
Copy No. 29 - R. M. Brick, Investigator, Research Project SR-109
Copy No. 107 - C. H. Lorig, Investigator, Research Project SR-110
Copy No. 108 - E. W. Suppiger, Investigator, Research Project SR-113
Copy No. 109 - E. R. Ward, Investigator, Research Project SR-113
Copy No. 110 - Carlo Riparbelli, Investigator, Research Project SR-113
Copy No. 111 - J. F. Wallace, Investigator, Research Project SR-114
Copy No. 20 - V. L. Russo, Investigator, Research Project SR-117
Copy No. 112 - R. A. Hechtman, Investigator, Research Project SR-119
Copy No. 113 - G. S. Mikhalapov, Investigator, Research Project SR-120
Copy No. 114 - Clarence Altenburger, Great Lakes Steel Company
Copy No. 115 - T. N. Armstrong, International Nickel Co., Inc.
Copy No. 116 - A. B. Bagsar, Sun Oil Company
Copy No. 117 - British Shipbuilding Research Association, Attn: J. C. Asher, Sec.
Copy No. 118 - George Ellinger, National Bureau of Standards
Copy No. 119 - A. E. Flanigan, University of California
Copy No. 120 - O. J. Horger, Timken Roller Bearing Company
Copy No. 121 - E. P. Klier, University of Maryland
Copy No. 122 - Robert C. Madden, Kaiser Steel Company
Copy No. 123 - N. M. Newmark, University of Illinois
Copies 124 thru 148 - E. G. Hill, British Joint Services Mission (Navy Staff)
Copy No. 149 - E. Orowan, Massachusetts Institute of Technology
Copy No. 150 - W. G. Perry, British Joint Services Mission (Navy Staff)
Copy No. 151 - L. J. Rohl, Carnegie-Illinois Steel Corp.
Copy No. 152 - W. P. Roop, Swarthmore College
Copy No. 153 - H. A. Schade, University of California
Copy No. 154 - Saylor Snyder, Carnegie-Illinois Steel Corp.
Copy No. 155 - Standard Oil Company of Calif., Attn: K. V. King
Copy No. 156 - Webb Institute of Naval Architecture
Copy No. 157 - Carl A. Zapffe, Carl A. Zapffe Laboratories
Copy No. 158 - Division of Metallurgy, National Bureau of Standards
Copy No. 159 - Transportation Corps Board, Brooklyn, New York
Copies 160 thru 164 - Library of Congress Via Bureau of Ships, Code 362
Copy No. 165 - NACA, Attn: Materials Research Coordination, Navy Department
Copy No. 166 - File Copy, Committee on Ship Steel
Copies 167 thru 171 - Bureau of Ships

Copy No. 172 - Dr. R. A. Hechtman - 2/21/51
Copy No. 173 - R. H. Raring - NRL - 5/6/51
Copy No. 174 - Rear Admn. W. C. Shepheard - 2/11/52 USCG
Copy No. 175 - Bethlehem Steel Co - 3/26/51
Copy No. 176 -
Copy No. 177 -
Copy No. 178 -
Copy No. 179 -
Copy No. 180 -
Copy No. 181 -
Copy No. 182 -
Copy No. 183 -

Copy No. 184 -
Copy No. 185 -
Copy No. 186 -
Copy No. 187 -} W. P. Rupp - 5/4
Copy No. 188 -}
Copy No. 189 - Nakagame, K. - Japan - 12-28-53
Copy No. 190 - Library - Bur. of Public Roads - 3-10-53
Copy No. 191 - Lockheed Aircraft Corp - Calif. — 8-14-56
Copy No. 192 -
Copy No. 193 -
Copy No. 194 -
Copy No. 195 -
Copy No. 196 -
Copy No. 197 -
Copy No. 198 -
Copy No. 199 -
Copy No. 200 -

D.C. Dawson 6/22/53
Library of Congress - 8/12/54
(Total Copies - 200)

Mr. A. J. Emmond, Lockheed Aircraft Corp., Burbank Calif. 2/24/55 - 1 copy
NAS-NRC (Library) ~~to~~ 8/10/56 - 1 copy
Dr. M. Maricek, - 1 copy - 3/4/58
Yugoslavia

Watertown Arsenal — attn: J. A. Talbot - 8/5/58

PROGRESS REPORT

NAVY BUSHIPS CONTRACT NObs-45521

PROJECT SR-98

A Study of Plastic Deformation and Fracturing by Strain Energy Distribution

Internally-Notched Steel Plates under Tension

by

S. I. Liu
Samuel T. Carpenter

Structural Laboratory
Swarthmore College
Division of Engineering
Swarthmore, Pa.

TABLE OF CONTENTS

ABSTRACT

This investigation was conducted to study the plastic deformation and fracturing of 12" wide, 3/4" thick internally notched steel plates under axial tension by determining the strain energy distribution on the surface of the deformed regions of the plates. Several stages in the process of deformation and fracturing at 70° F and 10° F were investigated to maximum load, 70° F being above the transition temperature, and 10° F being below the transition temperature. Surface strain energy distribution across the crack was also determined for a specimen fractured ductilely at 70° F.

By suing the octahedral theory in connection with the assumption of incompressibility and the assumption that the principal coordinate system is parallel to the three dimensions of the plate, the unit energies on the surface of the plate were obtained from grid measurements. By assuming that the energy distribution is independent of the thickness dimension, total energy is obtained for comparison with the total energy input measured from the load-elongation curve.

The results of this investigation show that the total energy based on octahedral theory and the above-stated assumptions agrees very well with the total observed energy input; that the rate of propagation of plastic deformation with respect to energy input decreases with decreasing temperature; that, for specimens with two dimensional similarity and constant thickness, the total energy of individual specimens of varying width can be predicted by the strain energy distribution of a single specimen of proper width; and that, at room temperature, the unit strain energy at the crack is found to be approximately in the order of 30,000 in-lbs per cubic inch in a ductile specimen.

LIST OF TABLES

LIST OF FIGURES

LIST OF FIGURES (continued)

LIST OF FIGURES (continued)

PROGRESS REPORT
NAVY BUSHIPS CONTRACT NObs-45521
PROJECT SR-98

A Study of Plastic Deformation and Fracturing by Strain Energy Distribution

Internally-Notched Steel Plates under Tension

by

S. I. Liu
Samuel T. Carpenter

Structural Laboratory
Swarthmore College
Division of Engineering
Swarthmore, Pa.

INTRODUCTION

Two of the most important factors which dictate the behavior of ship structure under service conditions are geometry and temperature. Many investigations have been undertaken in an effort to determine the effect of these two variables upon the flow and fracturing behavior of ship plate. Because of insufficient information on the physical insight of flow and fracturing phenomena generally, and in particular the transition phenomenon in steel, the problems involved are still far from a complete solution. However, the value of the mechanical and phenomenological approach to such problems has been demonstrated by the valuable applications in practice.

The effect of geometry operates through stress state. In most cases, experimental determination of plastic stress state is impossible. On the other hand, in many cases strain energy lends itself to measurements. Because of the possibility of measurement and because of the functional dependence between stress state and strain energy, one way to approach this problem is to deal with the effect of geometry in terms of "strain energy distribution".

Accordingly, this investigation was conducted to analyze the relation between the behavior of internally notched plates at various temperatures and the strain energy distribution developed under different stages of longitudinal tensile loading, by employing the octahedral theory in connection with grid measurements. By this means it may be ultimately possible to explain the effects of size and geometry on the basis of strain energy distribution. This preliminary investigation covers one plate size (12" wide by 24" long by 3/4" thick plate), one notch condition (a 3" internal slot with 0.023" end radius), two temperatures, 70° and 10° F, corresponding respectively to the ductile and cleavage fracture of this material. The grid analysis was studied for three specimens.

The results of this preliminary investigation are as follows. For identical specimens of constant thickness and two dimensional similarity under tension, it appears that the total strain energy absorbed at a stage of deformation after the first crack and after fracture can be predicted by considering the strain energy distribution of a single specimen of proper width. It was also found that as temperature decreases, the rate of propagation of deformation appears to decrease with respect to total strain energy input. For a ductile fracture, the unit strain energy at the fracture may be in the order of 30,000 in-lbs per cubic inch or greater. Under the geometric conditions investigated, the experimental results in terms of strain energy were found to be in good agreement with computations based upon the octahedral theory.

MATERIAL AND SPECIMENS

For this preliminary investigation, three 12" x 3/4" x 24" long steel plates of fully-killed "W" steel were used. The analysis of this material is given in Table I.

TABLE I

Chemical Analysis - "W" Steel

C	Mn	Si	Al	N
.21	.52	.23	.006	.005

Figure 1 shows the internally-notched specimen with lightly scratched 1/4" grid lines over a gage length of 9" on one surface of the plate. The 3" wide internal notch terminates in two holes of 0.046" diameter at the end of the jeweler's saw cut. To determine the unit energy near the crack, 1/16" grid lines were used for a single specimen tested to fracture at 70° F, the 1/16" grid lines extending to a longitudinal distance of 1½" from the transverse center line of the plate. The three specimens used, with testing and loading schedule, were as follows:

Specimen W-29-4: Tested at 70°F. Grid measurements made after the loads producing an observable crack at 0.046" dia. hole (277,000 lbs), 295,000 lbs, 325,000 lbs, and at a maximum load of 352,700 lbs. Approximately one week intervals between loadings after initial load.

Specimen W-29-3: Tested at 10°F. Grid measurements made after loads producing an observable crack at 0.046" dia. hole (277,740 lbs), 295,000 lbs, and at the fracture load of 325,000 lbs. Approximately one week intervals between loadings after initial load.

Specimen W-29-14: Tested continuously to fracture at a temperature of 70° F, and grid measured. See Figure 23 for load-elongation diagram.

Figure 2 shows the cylindrical specimen cut from the same material for the determination of the octahedral stress - octahedral strain function. The diameter is .650 ℄ .001". For measurement control, a notch of 2" radius and approximately .005" depth was machined on the cylindrical contour. The deviation from uni-axiality caused by such a very shallow notched-contour is assumed to be negligible.

PROCEDURE AND EQUIPMENT

Both types of specimen were welded to adapters. All testing was done in a 600,000 lb testing machine. The arrangements for maintaining temperature and for elongation measurements by a clip gage using SR-4 wire strain gages were described in detail in a previous paper.[1] * The temperature of 10° F was maintained by circulating air chilled by dry ice in an insulated transparent chamber surrounding the specimen. The grid deformations at different stages of loading were measured on a milling machine accurate to .001". All grid layouts were also measured before testing to provide a reference system. A time interval of about a week elapsed between unloading and reloading to allow for grid measurements.

The changes in diameter of the cylindrical specimens were measured by a mechanical strain gage accurate to .0001".

THEORY AND METHOD OF EVALUATION

As shown in Figure 1, a Cartesian system was chosen such that the x,y,z directions coincide with longitudinal, transverse and thickness dimensions of the plate. For convenience of measurement, the origin of the chosen coordinate system was put at the point O instead of the center of the plate.

According to octahedral theory,[2] the unit strain energy for any stress state is given by the following integral:

$$\omega = \frac{3}{2} \int \tau \, d\gamma \qquad (1)$$

---

* Superscripts refer to references in Bibliography

where u = unit strain energy in in-lbs/in^3

τ = octahedral shear stress in lbs/in^2

γ = octahedral shear strain

The local value of unit strain energy and the total strain energy for the gridded portion of the plate can be deduced from surface grid measurements by using Equation (1) and the following three assumptions:

(a) Constancy of volume (used in computing unit energy)

(b) The chosen x-y-z system is the principal system (used in computing unit energy)

(c) The unit strain energy is independent of z (used in computing total strain energy)

By the first two assumptions, the expressions for octahedral shear stress and octahedral shear strain are reduced to the following forms:

For uniaxial stress state:

$$\tau = \frac{\sqrt{2}}{3} S_x \tag{2}$$

$$\gamma = \sqrt{2}\, \varepsilon_x \tag{3}$$

For triaxial stress state:

$$\tau = \frac{1}{3}\sqrt{(S_x - S_y)^2 + (S_y - S_z)^2 + (S_z - S_x)^2} \tag{4}$$

$$\gamma = \sqrt{\frac{8}{3}}\sqrt{\varepsilon_x^2 + \varepsilon_x \varepsilon_y + \varepsilon_y^2} \tag{5}$$

where

S_x, S_y, S_z = principal stresses

$\varepsilon_x, \varepsilon_y$ = principal strains as given by:

$$\varepsilon_x = Ln(1 + e_x)$$
$$\varepsilon_y = Ln(1 + e_y) \tag{6}$$

where e_x, e_y = conventional strains as given by:

$$e_x = \frac{\partial U}{\partial x}$$
$$e_y = \frac{\partial V}{\partial y} \qquad (7)$$

where

U = displacement of a grid point in the x direction

V = displacement of a grid point in the y direction

The procedures for computing the surface unit strain energy from grid measurement are as follows:

(1) Establishing the "octahedral shear stress-octahedral shear strain" law by uniaxial test:

The true stress-strain relations before necking were obtained by tensile tests of the cylindrical specimens at 70° F and 10° F corresponding to ductile and cleavage fracture of the material in 12" wide internally notched plates, as shown in Figure 3. By Equation (2) and Equation (3), these true stress-strain data were expressed in terms of octahedral shear stress and octahedral shear strain with the quantity 3/2 (octahedral shear stress) as a dependent variable, as shown in Figure 4. The area under each curve in Figure 4 gives directly the unit strain energy.

(2) Establishing the relation between unit strain energy and octahedral shear strain:

By graphical integration of the two curves in Figure 4, the unit strain energy was plotted as functions of octahedral shear strain, as shown in Figure 5. These relations hold for any stress state according to octahedral theory. For large strains at 70° F, the unit strain energies were obtained from the experimental equation of the corresponding curve.

(3) Determining the local values of octahedral shear strain on the surface of the notched plate:

The grid measurements give the values of displacements (U and V) of the grid points in the x and y directions. The slope of the experimental curves, $U = f(x)$ and $V = f(y)$ gives corresponding conventional strains, which, by Equation (6), give the principal strains. By Equation (5), the principal strains were converted into octahedral shear strains.

(4) The surface unit strain energies were obtained by the universal relations (see equations 2 and 3) between unit strain energy and octahedral shear strain in Figure 5 and the octahedral shear strains determined in step (3).

Because of the second assumption that the shear strain components all vanish, the values of unit energy (U_o) in a small region in the vicinity of the notch and the crack are subjected to certain error. For this small region, the values of unit energy (U_o) should be multiplied by a factor to give the correct values (U):

$$U = U_o \left[1 + \frac{1}{4} \frac{\gamma_{xy}^2 + \gamma_{yz}^2 + \gamma_{zx}^2}{\varepsilon_x^2 + \varepsilon_x \varepsilon_y + \varepsilon_y^2} \right]^{\frac{n+1}{2}} \qquad (8)$$

where

U = unit energy based on all six strain components

U_o = unit energy based on the assumption that the x-y-z system used is the principal system

γ = shear strain components

n = strain-hardening exponent in uniaxial tension

As far as the total strain energy is concerned, neither the second nor the third assumption introduces any serious error, as has been confirmed by numerical evaluations.

Because of the preliminary data of the three plates investigated are not sufficient to correct the second assumption, all values of unit energy appearing in this report are values of U_o instead of U in Equation (8), but the difference between U_o and U is negligible except for a small region near the notch.

RESULTS AND DISCUSSION

Stress-Strain and Energy-Strain Relations of the Material:

The true stress-strain curves in uniaxial tension at 70° F and 10° F are shown in Figure 3. In Figure 4 the quantity 3/2 (octahedral shear stress) was plotted against octahedral strain so that the area under each curve gives directly the unit strain energy. Figure 5 shows the unit strain energy plotted as functions of the octahedral shear strain. All relations in these three figures show a slight effect of the temperature difference.

Macro-Propagation of Plastic Deformation and Strain Energy Distribution:

Figures 6 to 13 show by contours the unit strain energy distributions on the surface of the three specimens at various stages of loading. Figure 15 shows the distribution of unit energy absorbed between the first visible crack and fracture for specimen W-29-3 tested at 10° F. Except in Figures 10a and 10b, representing the results for the fractured specimen at 70° F, the energy distribution is approximately symmetrical with respect to the axes of symmetry of the specimen; however, the values of unit energy are average values of four quadrants, reported here as unit energy contours in one quadrant. Figure 14 shows the unit strain energy distribution in the diagonal and transverse directions at loads producing the visible crack for specimens W-29-4 and W-29-3. Figures 16 and 17 show the longitudinal distribution of unit strain energy across the crack after fracture at 70° F for specimen W-29-14.

Under the geometric conditions of the specimen, the primary direction of propagation of plastic deformation follows the diagonal extending from the end of the notch, as shown in Figures 6, 7, 8, 9, 11, 12 and 13. However, a secondary direction of propagation of deformation is developed in the direction of the advancing crack, when the crack propagates across the width of the specimen. This is more clearly revealed by the orientations of the unit energy contours representing the part of unit energy absorbed between the first visible crack and the fracture at 10° F as shown in Figure 15. These contours are primarily oriented in two directions; one follows the diagonal, and the other follows the width of the specimen. The former is due to the notch condition and probably has already been developed at the very early stage of the propagation of the crack; the latter results from the motion of the crack. As the crack proceeds, the propagation of plastic deformation mainly follows the direction of propagation of the crack; as a result, the orientation of the energy contours tends to become parallel to the crack, as revealed by the contours after fracture in Figures 10a and 10b. In no case investigated does the plastic zone cover the entire region within the gage lines.

At the loading producing the first visible crack, the energy contours, Figure 6, for specimen W-29-4 tested at 70° F and the energy contours, Figure 11, for specimen W-29-3 tested at 10° F may be compared. This comparison indicates that the specimen tested at 10° F had primarily a preference for deformation in the diagonal direction. A graphical comparison of unit energy variation in two directions along a 45° diagonal line extending from the notch toward the edge, and a transverse line extending from the notch outward, is given in Figure 14. At the next loading, 295,000 lbs., this preferential direction of deformation for specimen W-29-3 as defined by unit strain energy is largely eliminated. Figure 15 is a graphical representation of the way in which energy distribution is changed in the

specimen tested at 10° F during the loading interval between visible crack and the maximum load. The gain in energy absorption is primarily along two diagonal directions.

Specimen W-29-14 was tested continuously to fracture while maintaining a temperature of 70° F. Figures 10a and 10b show the computed energy contours at fracture for this specimen. It is to be noted that a single ridge of high energy absorption exists all along the fracture line, while a steep energy gradient exists as the crack is approached along all lines parallel to the vertical axis of the specimen. A plot of this energy variation is given in Figures 16 and 17. Although extrapolation of the energy data given in Figures 16 and 17 is undoubtedly an unscientific procedure, such extrapolations were made and a value of unit energy of about 30,000 in-lbs per cu.in. was obtained at the crack. This compares very poorly with values in the order of 90,000 to 100,000 in-lbs per cu.in. which may be expected at the crack.* In passing it may be said, however, that many of the grid points, where intersected by the crack, did show computed values of the order of 30,000 in-lb. per cu. in. These results hence point out the difficulties of the grid method in making such predictions even if extrapolation is carried out over such a short distance as a distance of 1/16".

Macro-Propagation of Plastic Deformation and the Crack:

The energy contours for 600 in-lb per cu.in. were selected to study the relation between total energy input and the extent of plastic zone. The value 600 in-lbs per cu. in. corresponds approximately to the value of octahedral shear strain at the end of "yielding jog", see Figure 4, in uniaxial tension. In Figure 18 the area swept by the 600 in-lbs contour was plotted as a function of

---

* Calculations based on theoretical strain energy conditions for fracture give a value of 90,000 in-lbs per cu.in. The University of California has reported unit energy values in the order of 150,000 in-lbs per cu. in. based on hardness surveys of the fracture zone.[5]

the total energy input. This figure reveals the following:

(1) The relation between the area swept by this contour and the total energy input appears to be linear.

(2) Extrapolation of the straight lines, Figure 18, apparently shows that the 600 in-lb contour may appear at the notch at the value of total energy input of approximately 10,000 in-lbs for both temperatures.

(3) The volume of metal undergoing plastic deformation appears to decrease with decreasing temperature.

To illustrate the macro-propagation of the crack itself, data that had been previously obtained on steel S-9[3] is presented in Figure 19. Two particular 12" wide specimens of this steel specimen, S-9-11 tested at 92° F with a ductile failure and specimen S-9-18 tested at 57° F with a cleavage failure were used in plotting Figure 19. The position of the end of the advancing crack measured from the notch has been plotted against the simultaneous energy input as measured by the area under the appropriate load-elongation diagram. The rate of propagation of the crack with respect to total energy input increases with decreasing temperature.

Theory and Experimental Facts:

In computing the unit and total energy from grid measurement, the octahedral theory has been used in conjunction with certain assumptions. It is not possible to experimentally check the degree of validity of each of the assumptions through unit energy. However, a comparison between the directly measured values of total energy input and the values of total energy obtained by integrating the local values from the grid measurement over the whole volume would give some indication as to the overall validity of the assumptions. In so doing, the following two aspects should be considered:

(1) The limit of integration for unit strain energy:

As shown in Figure 20, the value of unit energy at a value of octahedral shear strain (γ_1), measured after unloading, is actually computed to be a_1, whereas the unit energy input during the test loading cycle was $a_1 + a_2$. The energy calculated on the basis of experimentally determined strains is therefore less than the actual energy input by an amount a_2. Individual correction for a_2 is impossible; however, the total difference, Σa_2 for the entire plate can be corrected by the relation, $\Sigma\ a_2$ equals A_2, where A_2 equals the indicated part of total energy input from the load-deformation curve in Figure 20. A_2 is termed the error in strain energy integral, and represents the energy which must be added to the total energy calculated by the grid analysis to enable check comparisons to be made.

(2) Strain aging:

In the exploratory procedure of this investigation, it was necessary to allow about a week for grid measurement between unloading and reloading. This apparently caused strain aging as shown in Figures 21 and 22 where the load-elongation curves for the specimens W-29-4 and W-29-3 are compared with the load-elongation curves for similar specimens of "W" steel tested continuously. The load-deformation curves in these two figures show the two components of the effect of strain-aging:

(a) Increase in strength: For a given elongation, the load is higher in the strain-aged condition; therefore, the energy is higher by an amount measured by the area bounded by two load-deformation curves with and without strain aging. But the unit strain energies were computed from the stress-strain law in the absence of strain aging as shown in Figure 3.

(b) Decrease in ductility: As shown in these figures, the strain-aged specimen reached the maximum load at an elongation smaller than the elongation at the maximum load without strain-aging. Because of these two effects, the total energy computed from grid measurement under strain-aged conditions can only be compared to the total energy at the same elongation obtained from the load-elongation curves in the absence of strain-aging as for specimens W-32-7 and W-32-11 reported in a previous Progress Report.[3] (See Figures 21 and 22). These later specimens were run prior to the grid study and were deemed satisfactory for purposes of comparison. The reason for taking equal elongations for comparison is that for the same amount of elongation, the total amount of strain produced within the gage lines should be the same, no matter whether the specimen is strain-aged or not.

In case of the specimen W-29-14 tested continuously to complete fracture, the strain-aging effect does not appear; thus the value of total energy by grid measurement should be, and in fact is, very close to the directly measured values.

Table II lists a summary of energy computations for the three specimens used in the grid analysis. Before turning to this summary it is well to recall that two of the grid specimens W-29-3 and W-29-4 were subjected to strain-aging during the process of the investigation. It must also be recalled that the error A_2 in the strain energy integral must be taken into account when making comparisons between computed energies by the grid analysis and measured energy input. These combined effects make it impossible to directly compare the total energy input for the specimens which were strain-aged with the strain energy corrected for the error A_2. As a consequence, specimen W-32-11 has been

TABLE II

Summary of Energy Computations

Col. 1 Applied Load, lbs	Total Energy Input by Load-Elongation Curve - in-lbs. Col. 2 With strain-aging (Spec. W-29-4 at 70°)	Col. 3 Without strain-aging Spec. W-32-7 at 81°)	Total Grid Energy Based on Octahedral Theory - in-lbs. Col. 4 Before correction for error in strain energy integral	Col. 5 Corrected for error in strain energy integral
Ductile Fracture				
277,000 (visible crack)	23,560* (no strain-aging)	23,700*	21,356	23,966**
295,000	24,420	24,480*	23,304	26,702**
325,000	52,580	50,360*	44,792	48,712**
352,700 (Max.load)	78,500	73,340*	70,488	74,878**
Cleavage Fracture	(Spec. W-29-3 at 10°)	(Spec. W-32-11 at 21°)		
277,740 (visible crack)	17,920* (no strain aging)	--	14,888	17,888**
295,000	21,800	21,600*	19,134	25,034**
325,000 (max.load)	35,320	34,460*	31,251	36,151**
		(Spec. W-29-14 tested continuously at 70°)		
		265,000*	256,785	260,085**

(*, **): Figures with (*) are comparable with corresponding figures with (**).

used for comparing the results of W-29-3, and specimen W-32-7 has been used for comparing the results of W-29-4. Accordingly the values of energy shown in column 3 and column 5 of Table II are comparable. Note that no additional specimen was needed to compare the results of specimens W-29-14 since strain aging was not present. In addition, the energy shown in column 2 for the visible crack loadings is also comparable with column 5 since during the first loading of the specimens to the visible crack load no strain-aging effects appear. The degree of correlation between the values in column 3 and column 5 of Table II is clearly shown in Figure 24, where the directly measured values of total energy input agree closely with the values of total energy by grid measurements when properly corrected for strain-aging and the error in the strain energy integral. This agreement indicates that the assumptions are substantially correct. Near the notch exceptions would need to be made, as no elementary considerations would probably hold in this region.

Correlation with Specimen of Varying Width and Constant Thickness:

For the following listed reasons, it seems possible that the energy absorption of individual specimens of various width but of the same thickness can be predicted by using the energy distribution found in the 12" wide specimens:

(1) The unit energy at the crack is the same regardless of width of specimen after failure by ductile behaviour.

(2) At the end of the advancing crack, the notch acuity (and therefore the stress state) is essentially the same regardless of the width of the specimen.

It follows from the first reason that at given temperature and a given stage of straining, the energy surfaces, $u = f(x,y)$ for specimens of varying width have an equal maximum at the crack; and it follows from the second reason

that the energy surfaces for specimens of varying width fall off from an equal maximum value at approximately equal slopes. This leads to the deduction that each half of a narrow specimen might behave as if it were a part of a wide specimen, if the notch-ends of both specimens were made coincident.

The first step in examining this deduction was to construct Figure 25, as follows:

> Upon the surface of the 12" wide fully ductile specimen W-9-4, there has been drawn the outlines of one quadrant of 3/4" thick internally notched plates, each of different aspect ratio. Aspect ratio, designated by "AR", is equal to width divided by thickness. The ends of the notches were all made coincident with each other as shown in Figure 25. The quadrant referred to has dimensions equal to one half the width of the plate, and a length equal to one half the gage length where the gage length is three fourths the width of a given specimen.

The next step in comparing the plates as shown in Figure 25 was to compute average unit strain energies at maximum load termed (u'). Average unit strain energy (u') was obtained by first calculating the total strain energy within the boundaries of one quadrant of a plate for a given (AR) and dividing this total energy by the volume of metal in one quadrant of the plate. The total strain energy was determined by utilizing the unit strain energy distribution as given in Figure 9 for the fully ductile specimen W-29-4 at maximum load. This was separately done for various values of AR varying from 16 for the 12" wide specimen to an AR of 1 for the narrowest plate considered. The derived values of the unit energies (u') are plotted in Figure 26.

Independently of the foregoing procedure, the average unit energies (u) at maximum load of individual 3/4" thick ductile specimens of 3,6, and 12" widths of "W" steel (previously tested, but not reported in detail here) were determined. These unit energies (u) are plotted in Figure 26. To obtain values of (u) at maximum load for greater width, data given in the final report[4] of the University of Illinois for "D" steel, fully killed, and chemically similar to "W" steel, have also been plotted. University of Illinois specimens, 18B-3 of 24" width (AR=32) and 17A-7 of 72" width (AR=96) were the only two complying with the requirement needed here, namely, fully ductile action. The dotted extension of the (u) curve should only be considered as tentative and indicative that grid analysis for 12" wide specimens might possibly be of use in predicting total energy or unit energy for wider plates. Further tests at larger aspect ratio are needed to confirm this statement.

Figure 26 shows two curves, one marked (u') and the other marked (u). The difference in unit energy between these two curves may be attributed to second effect of strain-aging (see page 12). The (u') values were obtained from the 12" specimen W-29-4 which had undergone strain-aging while the (u) values were obtained from specimens continuously tested. For a 12" wide specimen (AR=16) continuously tested, data was available to compare total energies at equal elongation over the gage length of 9". The value of (u) for AR 16 was reduced to a value comparable to (u') by using the area under the load-elongation curve at the elongation reached by specimen W-29-4 at maximum load. This reduced value is plotted as a hollow square and agrees with the value of (u') obtained for W-29-4 in the presence of strain-aging. This indicates that, should the specimen used for grid measurement be loaded to maximum load without strain-aging, the (u') curve would tend to coincide with the (u) curve.

The same procedure was also extended to the fully ductile specimen W-29-14 which was tested continuously to fracture. The strain energy distribution after fracture, shown in Figure 10a, then forms the basis for computing average

unit energy within the gage length volume. The outlines of plates of varying aspect ratio are superimposed on Figure 10a by the method indicated by Figure 25. The unit energy values derived from Figure 10a are plotted in Figure 27, giving the upper curve. For comparison with the upper curve, two points have been plotted representing actual test results for aspect ratios of 4 and 8, in addition to the experimentally determined value at AR 16. The derived curve and the test results agree closely. The lower curve of Figure 27 is the (u') curve of Figure 26 representing unit energy to maximum load. It appears that the upper and lower curves tend to intersect at low aspect ratios. This is perhaps explained by the fact that, once the crack goes through a part of the specimen, that part is subjected to very little additional plastic deformation as the crack advances further.

The correlations noted in Figures 26 and 27 strongly suggest that the strain energy distribution of a single specimen of proper width and thickness can be used to predict the energy absorption of individual plates of varying width and thickness.

CONCLUSIONS

Analysis of the experimental data of these specimens at this exploratory stage show primarily:

(1) that the use of octahedral theory is confirmed in terms of strain energy by the results of this investigation.

(2) that the strain energy distribution of a single specimen of proper width appears useful in predicting the total energy of individual specimens of varying width and constant thickness.

(3) that, as temperature decreases, the rate of propagation of deformation with respect to total strain energy input decreases, and the rate of propagation of crack with respect to total strain energy input increases.

(4) that, for ductile action, the unit strain energy at the crack is found to be approximately in the order of 30,000 in-lbs per cu.in.; however, this value may be questionable in view of extrapolation methods used.

SUGGESTED FUTURE WORK

The experimental results described suggest future work in the following directions:

(1) Changing the experimental procedure to eliminate strain-aging and to obtain more complete data. To this end, a method of photographing the grids at intermediate loads is preferable, so as to permit continuous loading to fracture.

(2) Investigating the strain energy distribution in the entire range from yielding to fracture, for both shear and cleavage failures, to reveal the macro-mechanism of the whole process.

(3) Investigating specimens of different size at different temperatures. The material for investigation should be chosen so that previous data will be available to compare with the results of grid analyses.

(4) Experimental and theoretical analysis for the small region around the notch.

ACKNOWLEDGEMENTS

The detail work of this investigation was performed by Dr. S. I. Liu, Research Associate, in collaboration with and under the general supervision of Professor Samuel T. Carpenter, Chairman, Department of Civil Engineering. The helpful advice of W. P. Roop (Captain, USN, Retired) is also acknowledged.

Mr. Ewald Kasten contributed greatly to the instrumentation for measuring the grids and the tests were made under the supervision of Mr. A. W. Zell. Drawings were made by Erwin Newman and Roy Bosshardt.

BIBLIOGRAPHY

(1) S. T. Carpenter, W. P. Roop, et al, Swarthmore College, Swarthmore, Pa. "Progress Report on Twelve-Inch Flat Plate Tests", Ship Structure Committee Report, Serial No. SSC-21, April 15, 1949.

(2) A. Nadai, "Energy of Distortion absorbed by Plastic Deformation of Thin Steel Plates". Research Report SR-182, Westinghouse Research Laboratories, April 1943.

(3) S. T. Carpenter, W. P. Roop, E. Kasten and A. Zell, Swarthmore College, Swarthmore, Pa., "Progress Report: Part I Twelve Inch Flat Plate Tests, Part II Aspect Ratio Program", Ship Structure Committee Report Serial No. SSC-35, December 15, 1949.

(4) W. M. Wilson, R. A. Hechtman and W. H. Bruckner, University of Illinois, "Final Report on Cleavage Fracture of Ship Plates as Influenced by Size Effect", Ship Structure Committee Report, Serial No. SSC-10, June 12, 1947.

(5) H. E. Davis, G. E. Troxell, A. Boodberg, E. R. Parker and M. P. O'Brien, University of California Progress Report on "Causes of Cleavage Fracture in Ship Plate: Flat Plate Tests", Ship Structure Committee Report, Serial No. SSC-2, August 23, 1946.

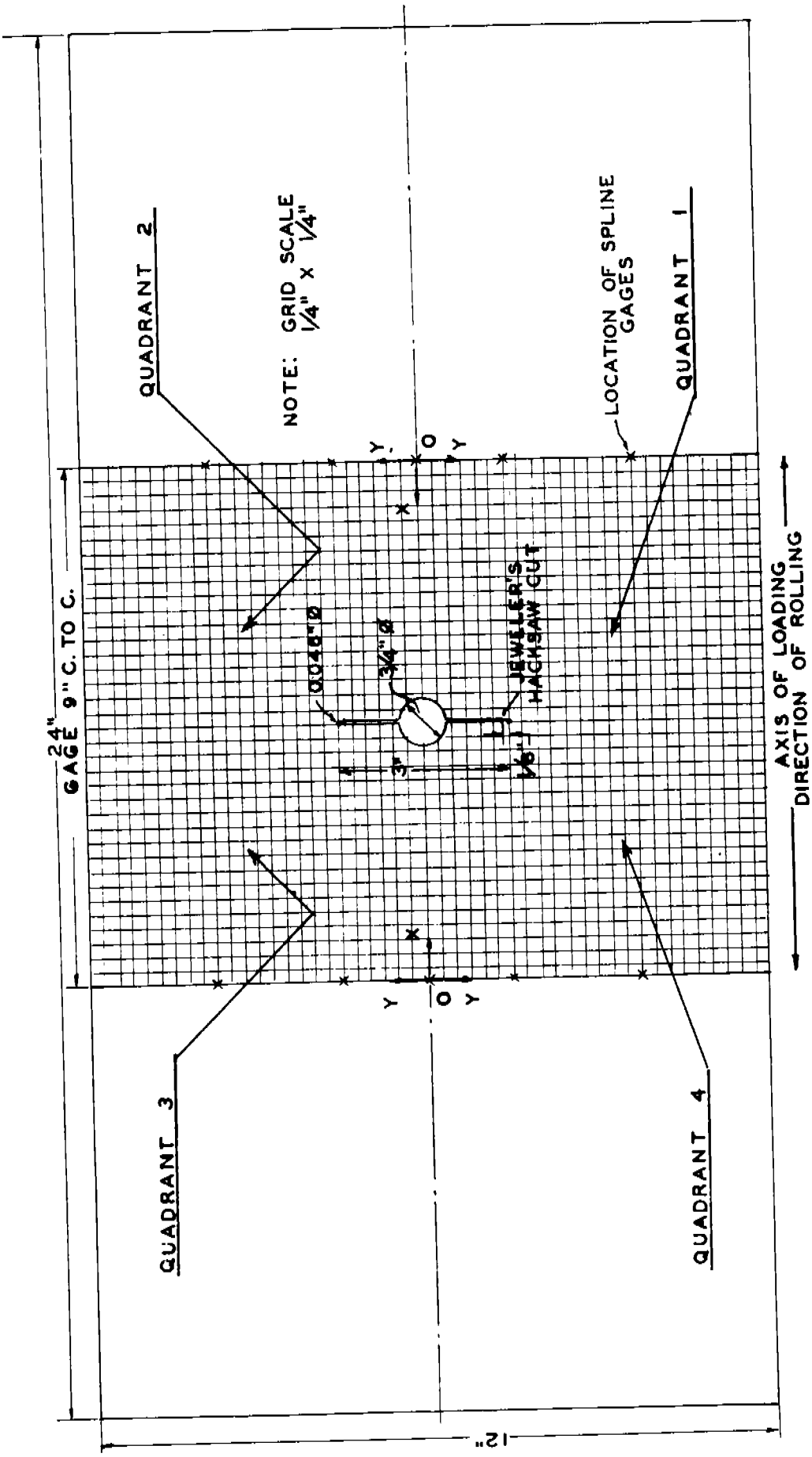

FIG. 1 TEST SPECIMEN FOR STRAIN ENERGY DISTRIBUTION

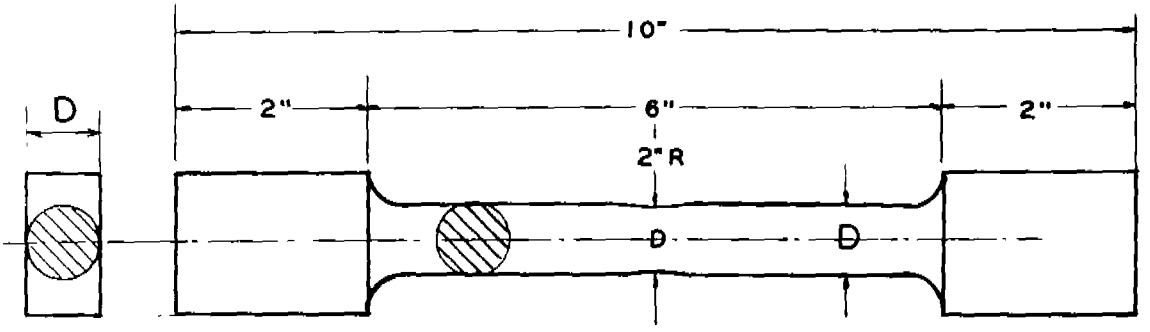

FIG. 2 TEST SPECIMEN FOR UNI-AXIAL TENSION

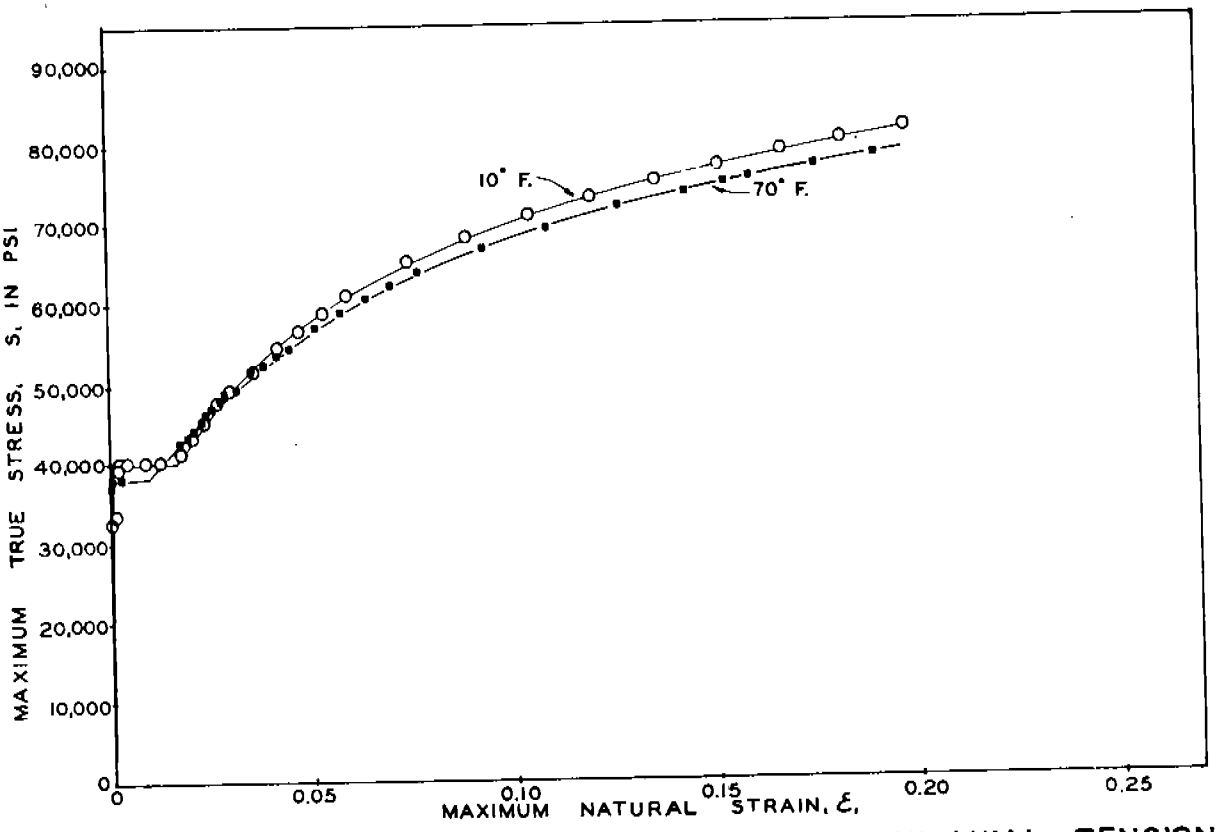

FIG. 3 TRUE STRESS-STRAIN CURVES IN UNI-AXIAL TENSION

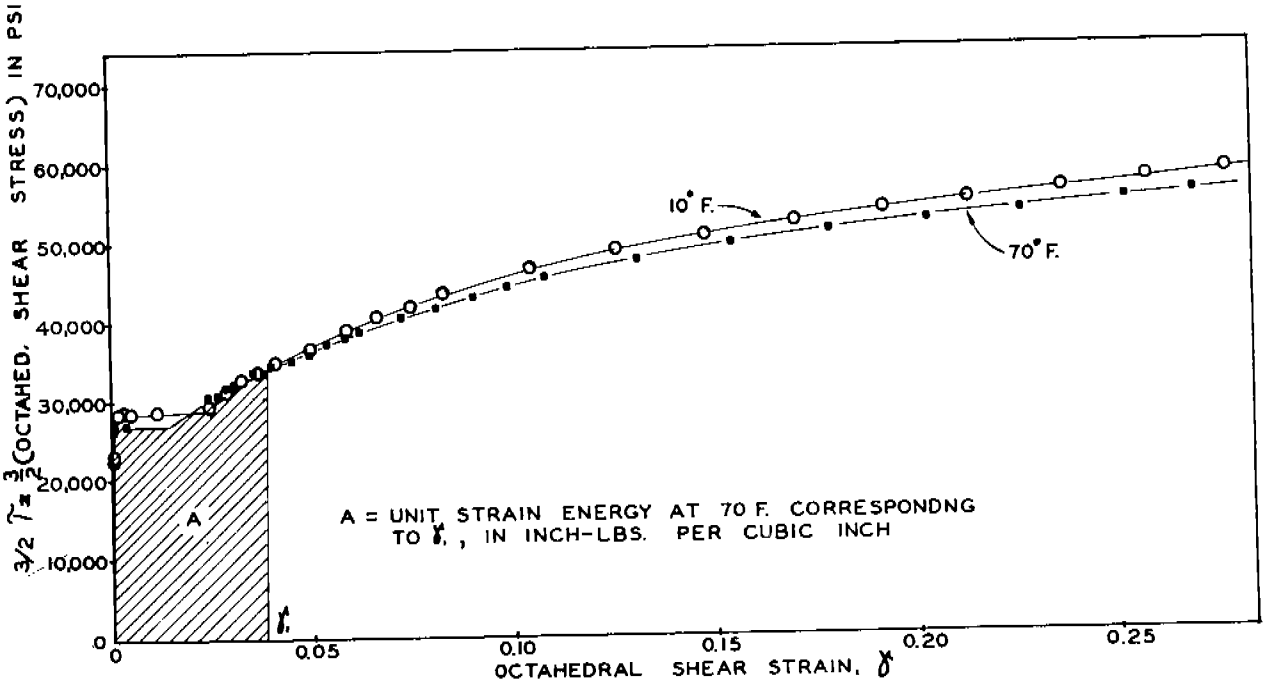

FIG. 4 UNIVERSAL STRESS-STRAIN FUNCTIONS FOR 3/4" W-STEEL SHIP PLATE

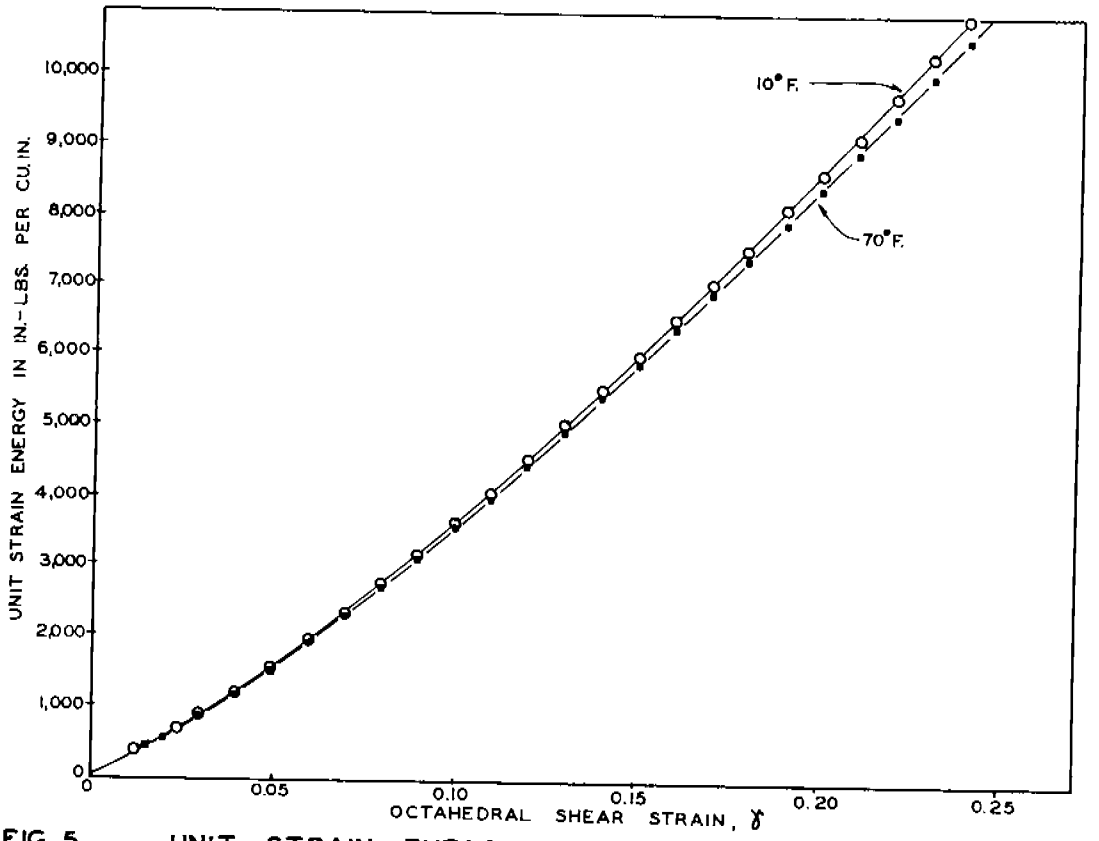

FIG. 5 UNIT STRAIN ENERGY OF 3/4" SHIP PLATE AS FUNCTIONS OF OCTAHEDRAL SHEAR STRAIN AS DETERMINED BY UNI-AXIAL TEST AT 70°F. AND 10°F.

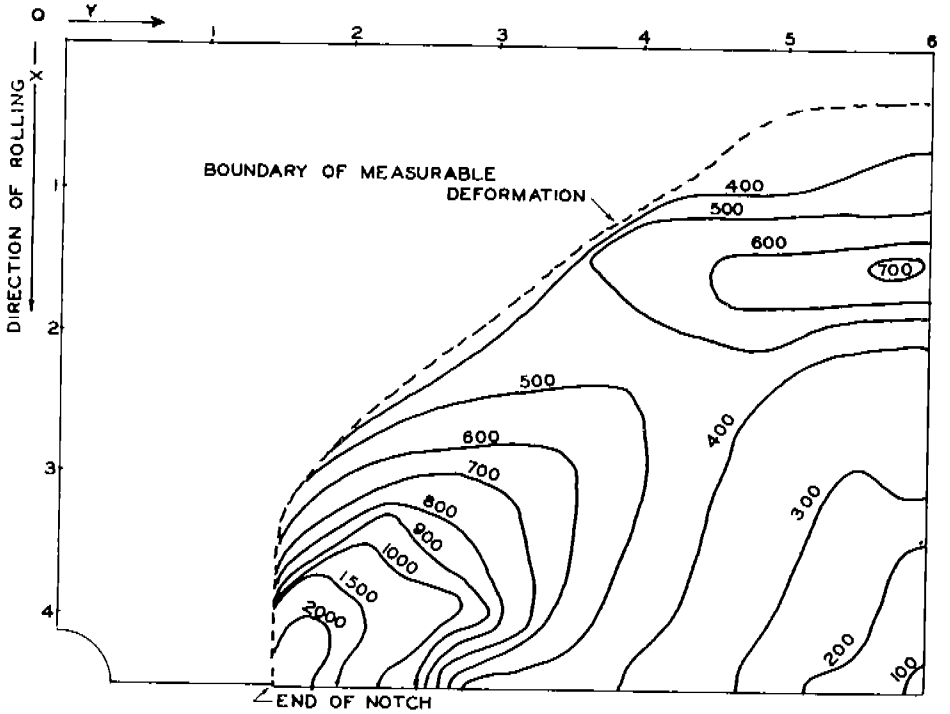

FIG. 6 UNIT STRAIN ENERGY DISTRIBUTION ON THE SURFACE OF A 12" X 3/4" NOTCHED SPECIMEN, W-29-4, LOADED TO 277,000 LBS. (VISIBLE CRACK) AT 70° F.

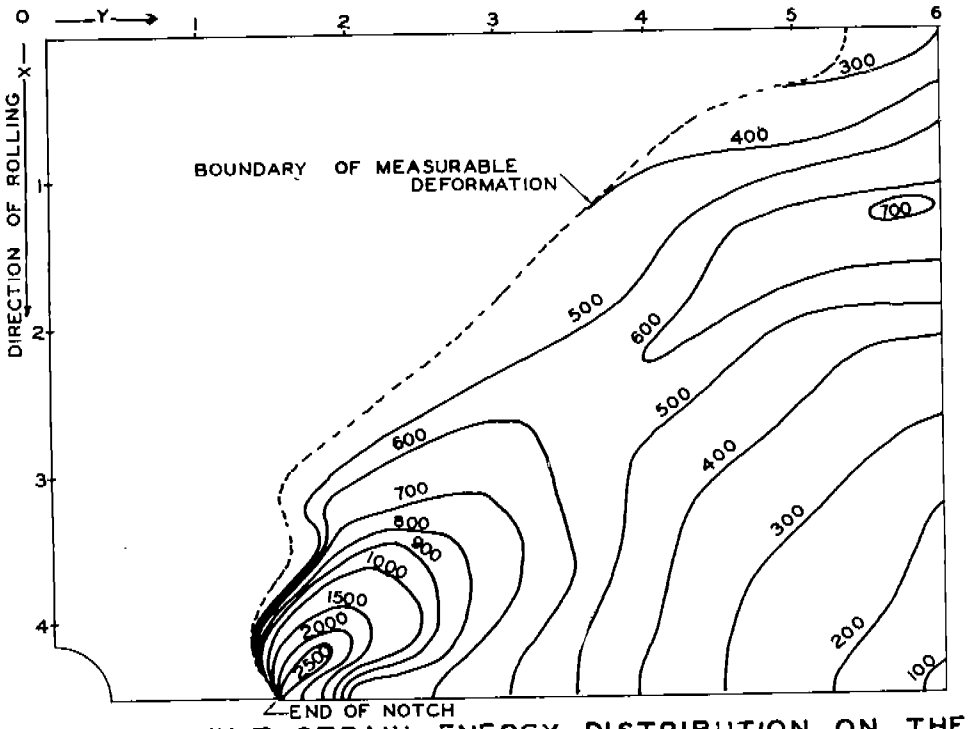

FIG. 7 UNIT STRAIN ENERGY DISTRIBUTION ON THE SURFACE OF A 12" X 3/4" NOTCHED SPECIMEN, W-29-4, LOADED TO 295,000 LBS. AT 70° F.

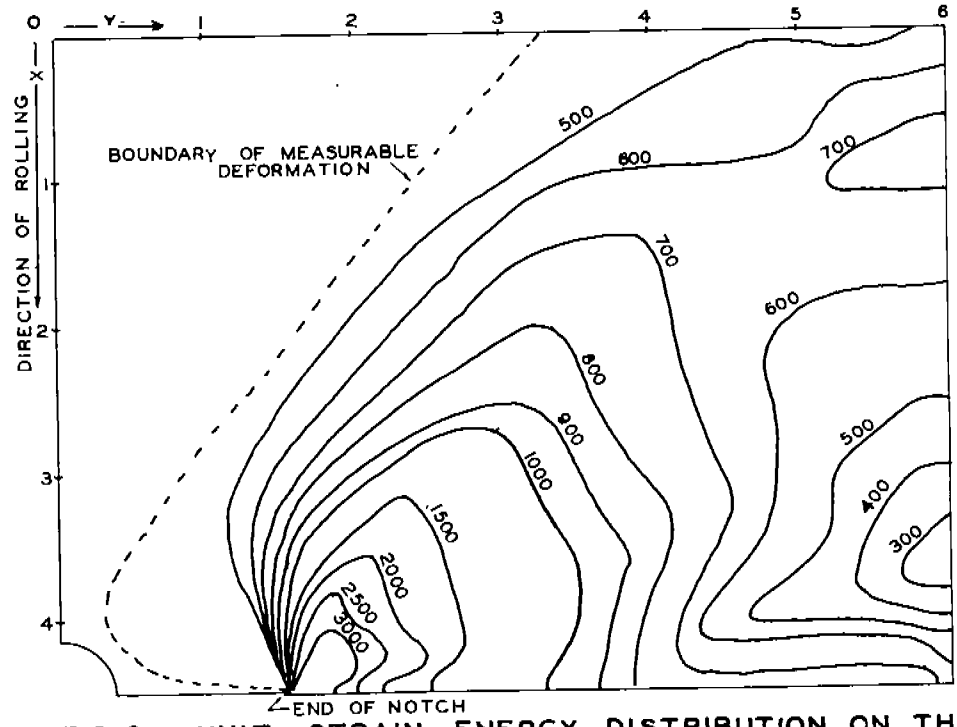

FIG. 8 UNIT STRAIN ENERGY DISTRIBUTION ON THE SURFACE OF A 12" X 3/4" NOTCHED SPECIMEN, W-29-4, LOADED TO 325,000 LBS. AT 70° F.

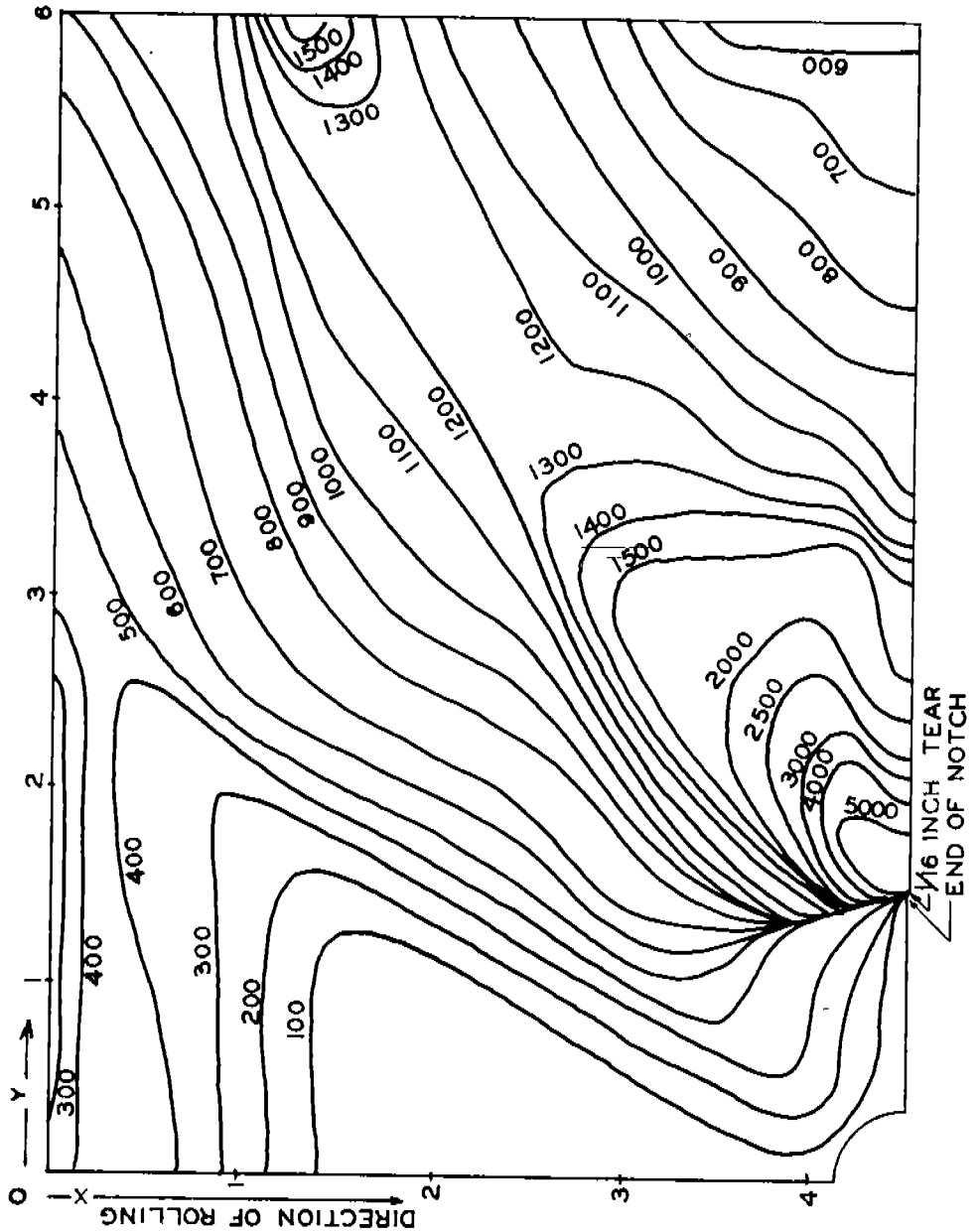

FIG. 9 UNIT STRAIN ENERGY DISTRIBUTION ON THE SURFACE OF A 12" X 3/4" NOTCHED SPECIMEN, W-29-4, LOADED TO 352,700 LBS. MAX. LOAD AT 70° F.

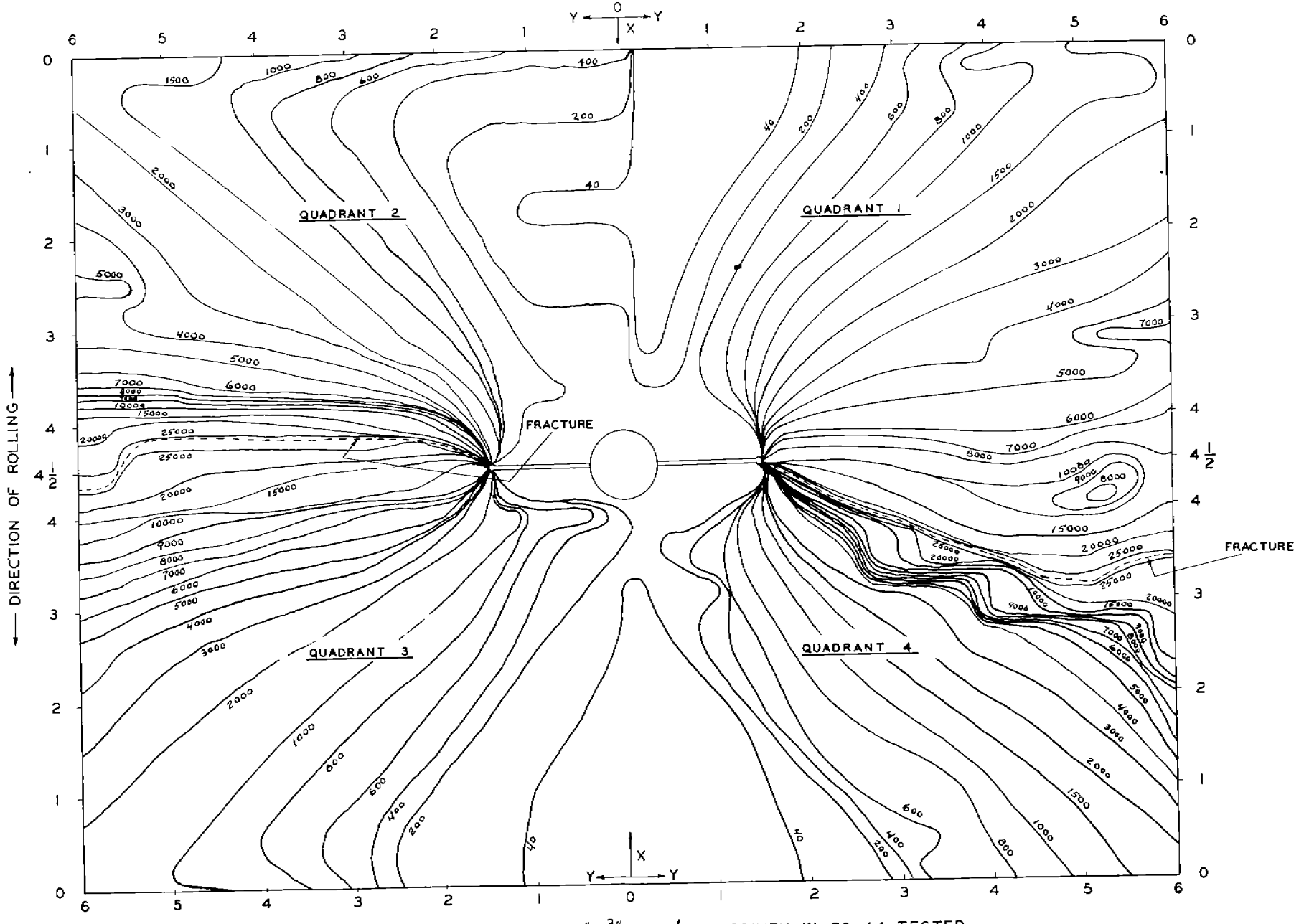

FIG. 10_A UNIT STRAIN ENERGY DISTRIBUTION ON THE SURFACE OF A 12" X $\frac{3}{4}$" NOTCHED SPECIMEN, W-29-14, TESTED TO FRACTURE AT 70°F. (X,Y IN INCHES).

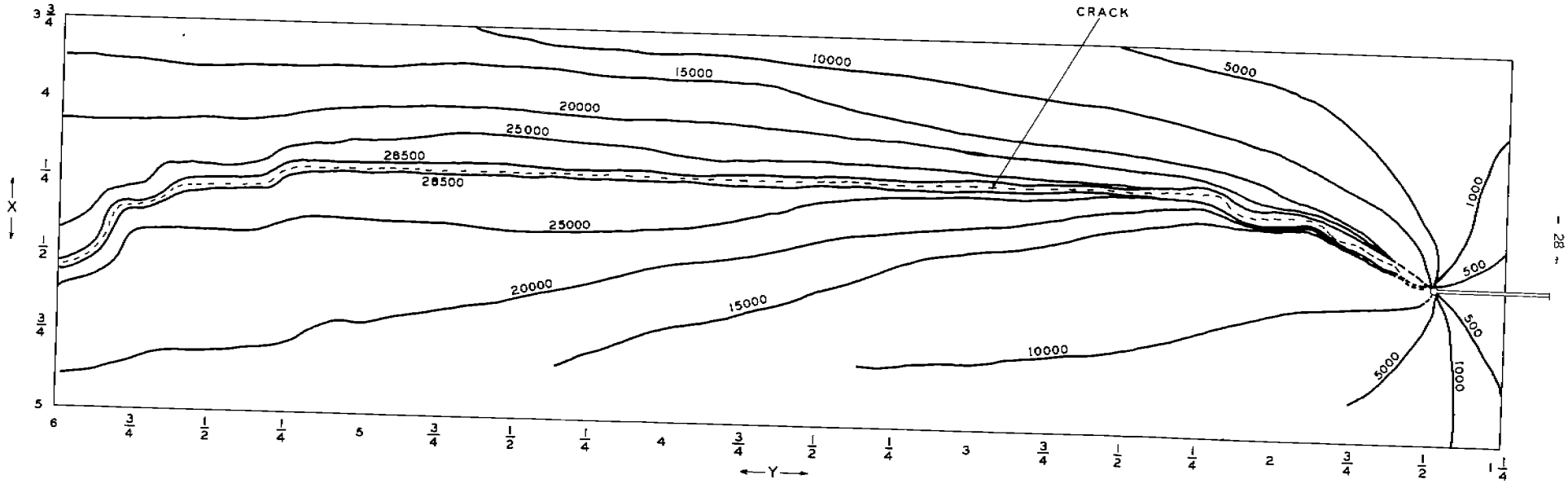

FIG. 10_B UNIT STRAIN ENERGY DISTRIBUTION NEAR THE CRACK ON THE SURFACE OF A 12"X3/4" NOTCHED SPECIMEN, W-29-14, TESTED TO FRACTURE AT 70°F. (X,Y, IN INCHES) — QUADRANT 2 AND 3.

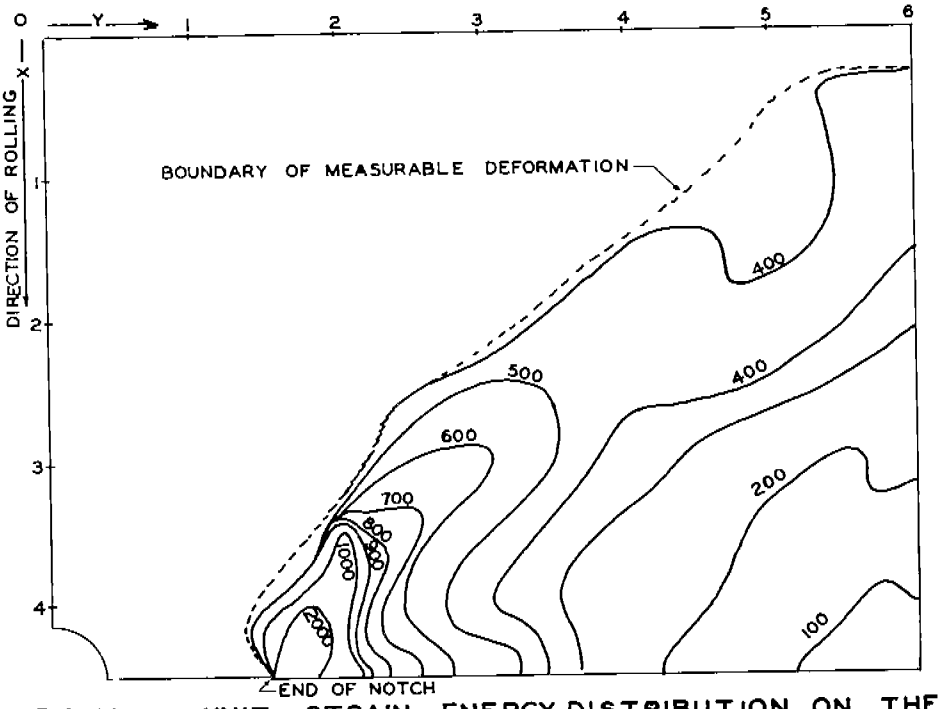

FIG. 11 UNIT STRAIN ENERGY DISTRIBUTION ON THE SURFACE OF A 12" X 3/4" NOTCHED SPECIMEN, W-29-3, LOADED TO 277,740 LBS. (VISIBLE CRACK) AT 10° F.

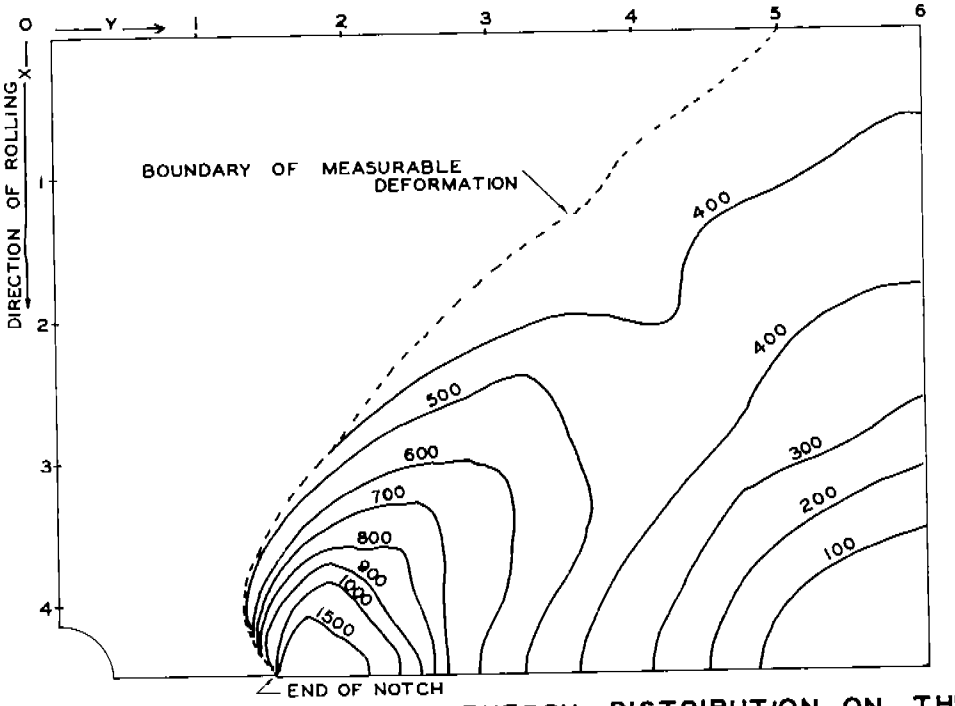

FIG. 12 UNIT STRAIN ENERGY DISTRIBUTION ON THE SURFACE OF A 12" X 3/4" NOTCHED SPECIMEN, W-29-3, LOADED TO 295,000 LBS. AT 10° F.

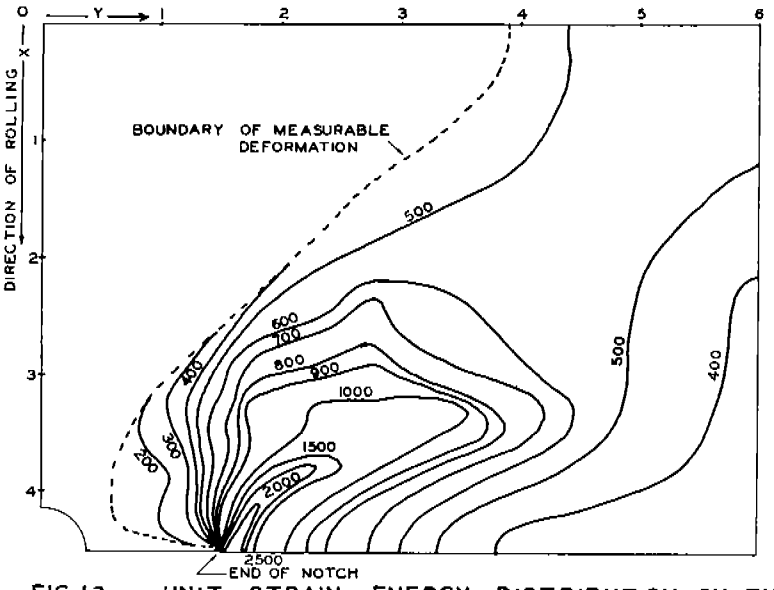

FIG. 13 UNIT STRAIN ENERGY DISTRIBUTION ON THE SURFACE OF A 12" X 3/4" NOTCHED SPECIMEN, W-29-3, LOADED TO 325,000 LBS. (FRACTURE) AT 10° F.

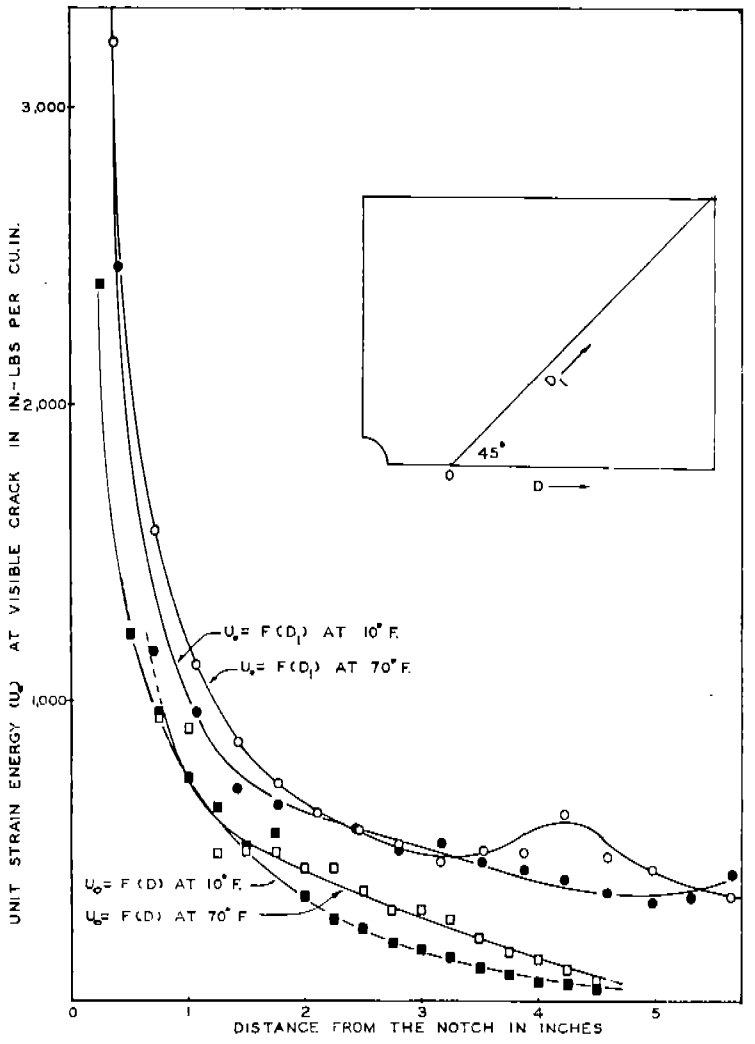

FIG. 14 UNIT STRAIN ENERGY DISTRIBUTION IN THE DIAGONAL (D_1) AND TRANSVERSE (D) DIRECTION OF 12" X 3/4" NOTCHED SPECIMENS LOADED TO VISIBLE CRACK AT 70° F. AND 10° F.

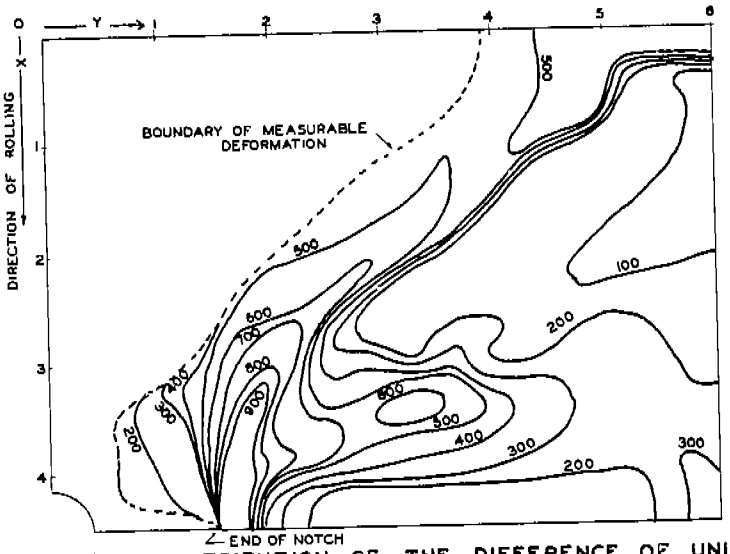

FIG. 15 DISTRIBUTION OF THE DIFFERENCE OF UNIT STRAIN ENERGIES FROM 277,740 LBS. (VISIBLE CRACK) TO 325,000 LBS. (FRACTURE) FOR THE 12" X 3/4" NOTCHED SPECIMEN, W-29-3, AT 10° F.

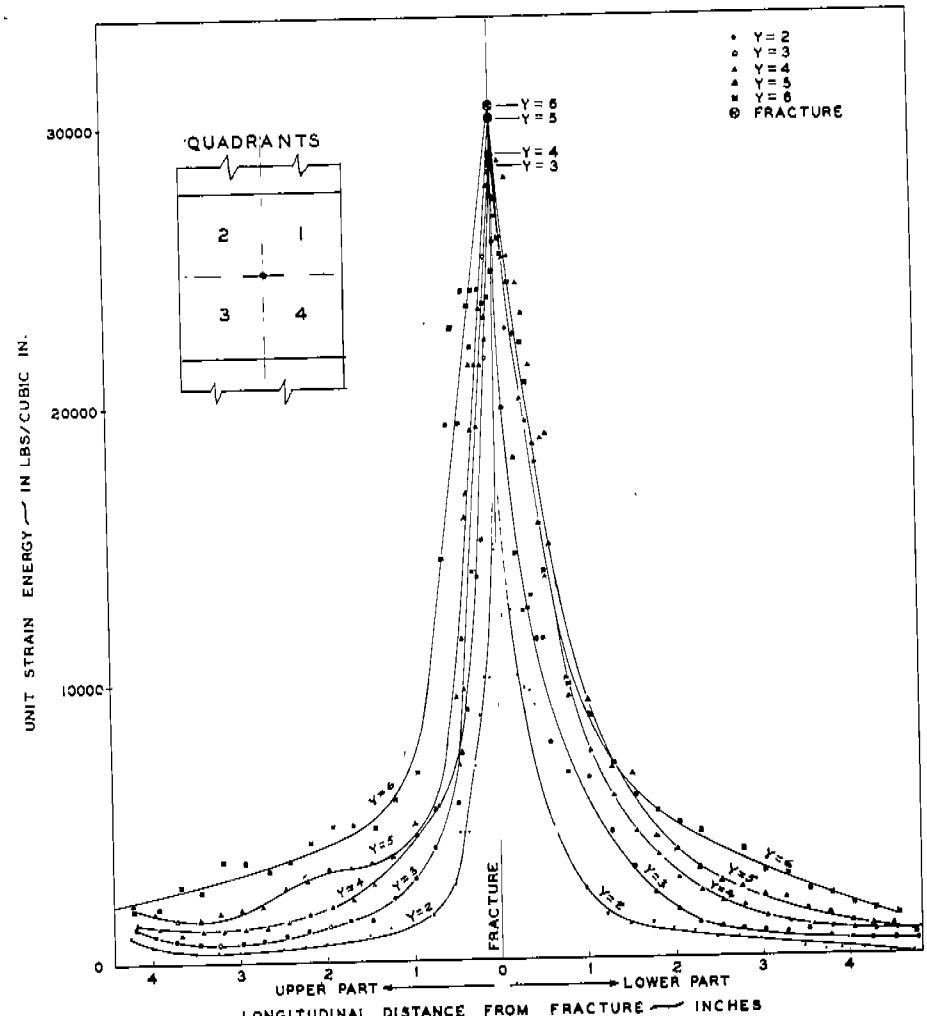

FIG. 16 LONGITUDINAL DISTRIBUTION OF UNIT STRAIN ENERGY ON THE SURFACE OF A 12"X3/4" NOTCHED SPECIMEN, W-29-14, TESTED TO FRACTURE AT 70°F. QUADRANTS 2 AND 3.

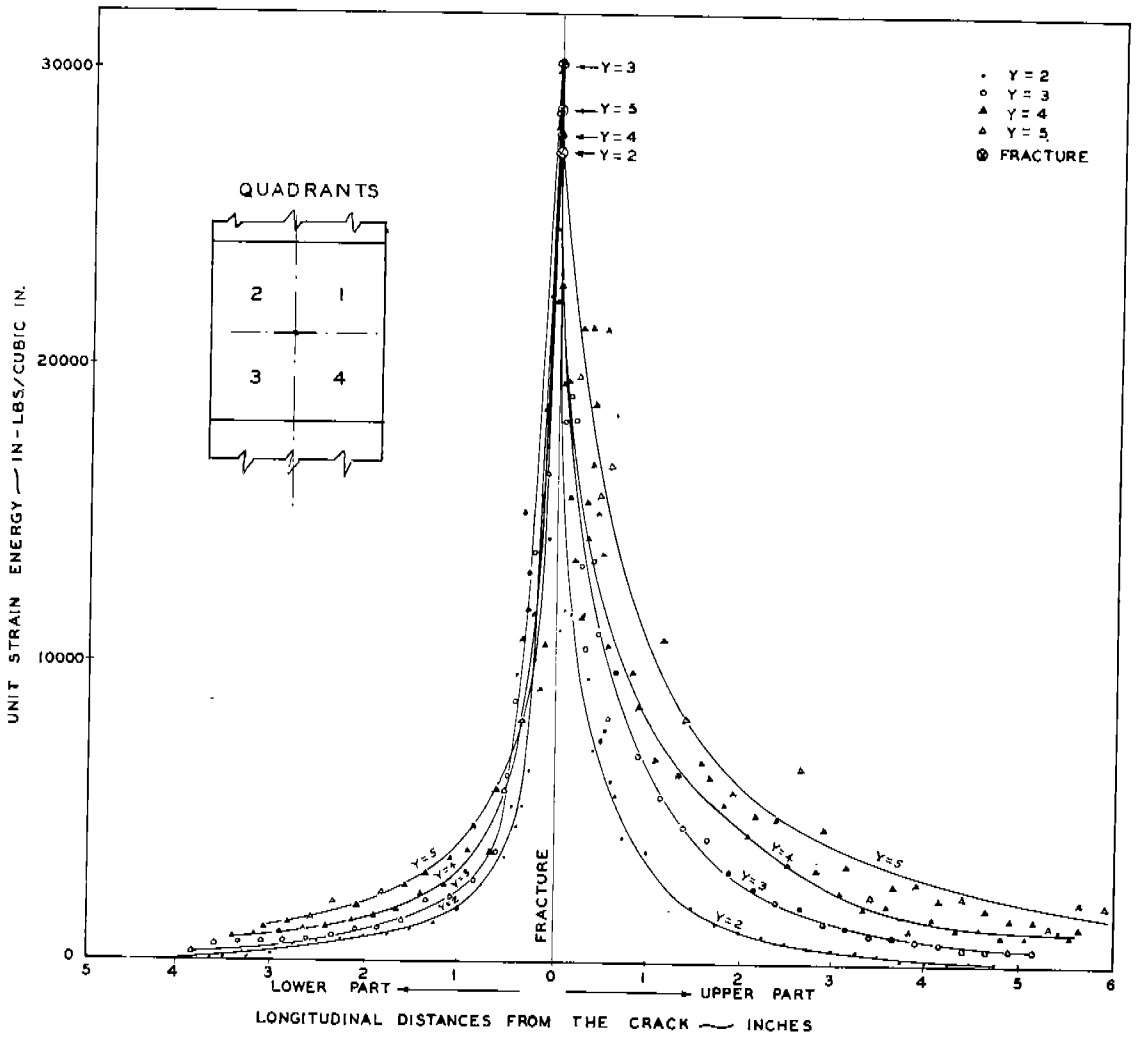

FIG 17 LONGITUDINAL DISTRIBUTION OF UNIT STRAIN ENERGY ON THE SURFACE OF A 12"X 3/4" NOTCHED SPECIMEN, W-29-14, TESTED TO FRACTURE AT 70°F. QUADRANTS 1 AND 4

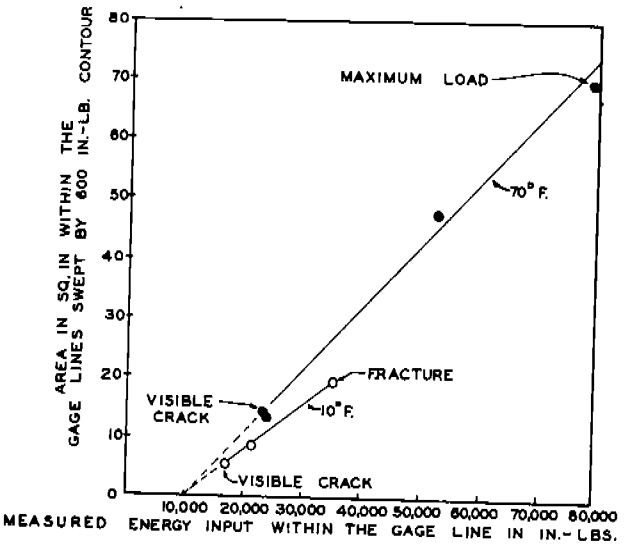

FIG. 18 MACRO-PROPAGATION OF PLASTIC DEFORMATION WITHIN 12" X 3/4" NOTCHED SPECIMENS UNDER LONGITUDINAL TENSION AT 70°F. AND 10°F.

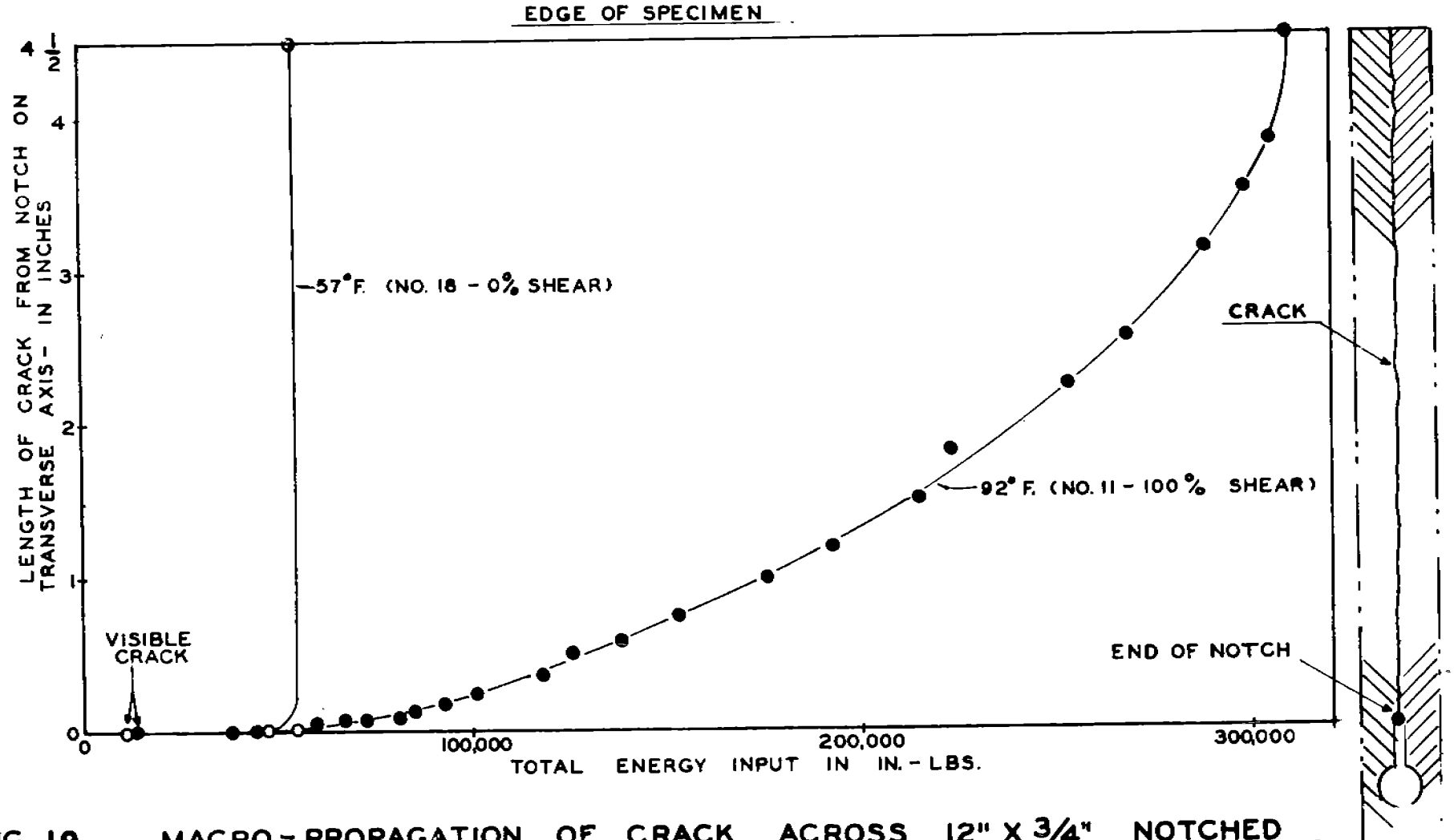

FIG. 19 MACRO - PROPAGATION OF CRACK ACROSS 12" X 3/4" NOTCHED SPECIMENS OF STEELS S-9 - NO. 11 AT 92° F. AND S-9 - NO. 18 AT 57° F., CORRESPONDING TO DUCTILE AND BRITTLE FRACTURES

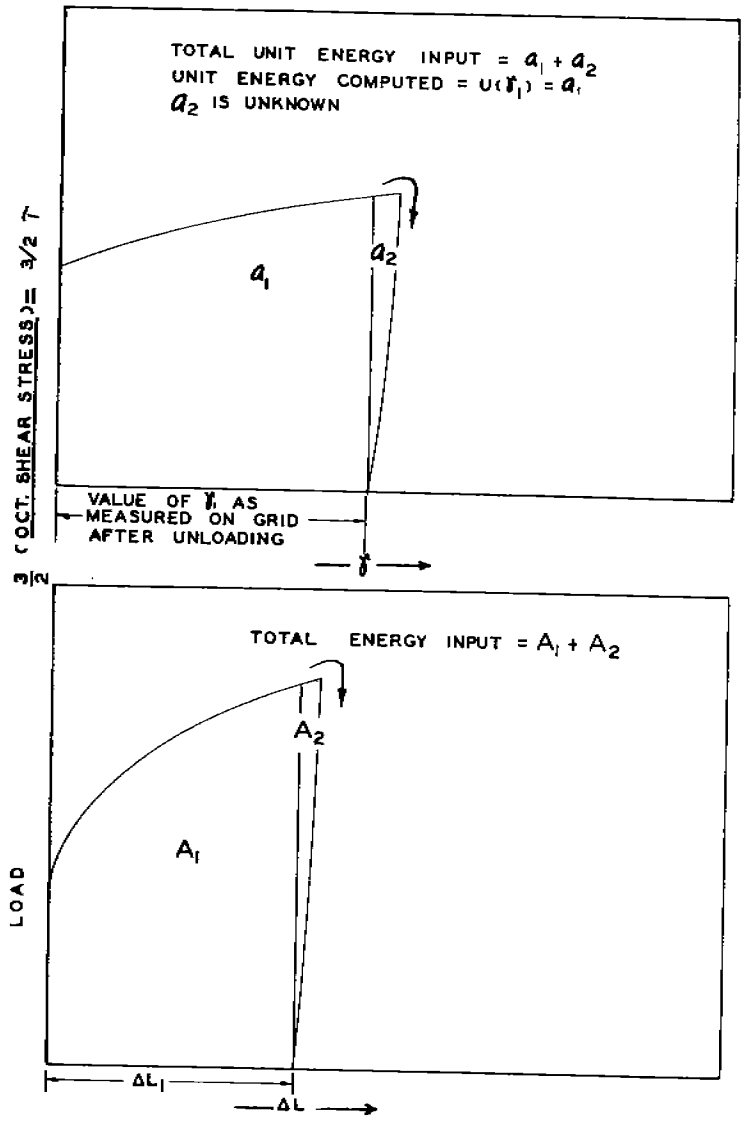

(1) Σa_1 FOR THE ENTIRE PLATE (I.E., THE TOTAL GRID ENERGY AS COMPUTED) DOES NOT CORRESPOND TO THE TOTAL ENERGY INPUT, $A_1 + A_2$

(2) CORRECTION: Σa_2 (FOR WHOLE PLATE) = A_2

FIG. 20 ERROR IN STRAIN ENERGY INTEGRAL AND ITS CORRECTION

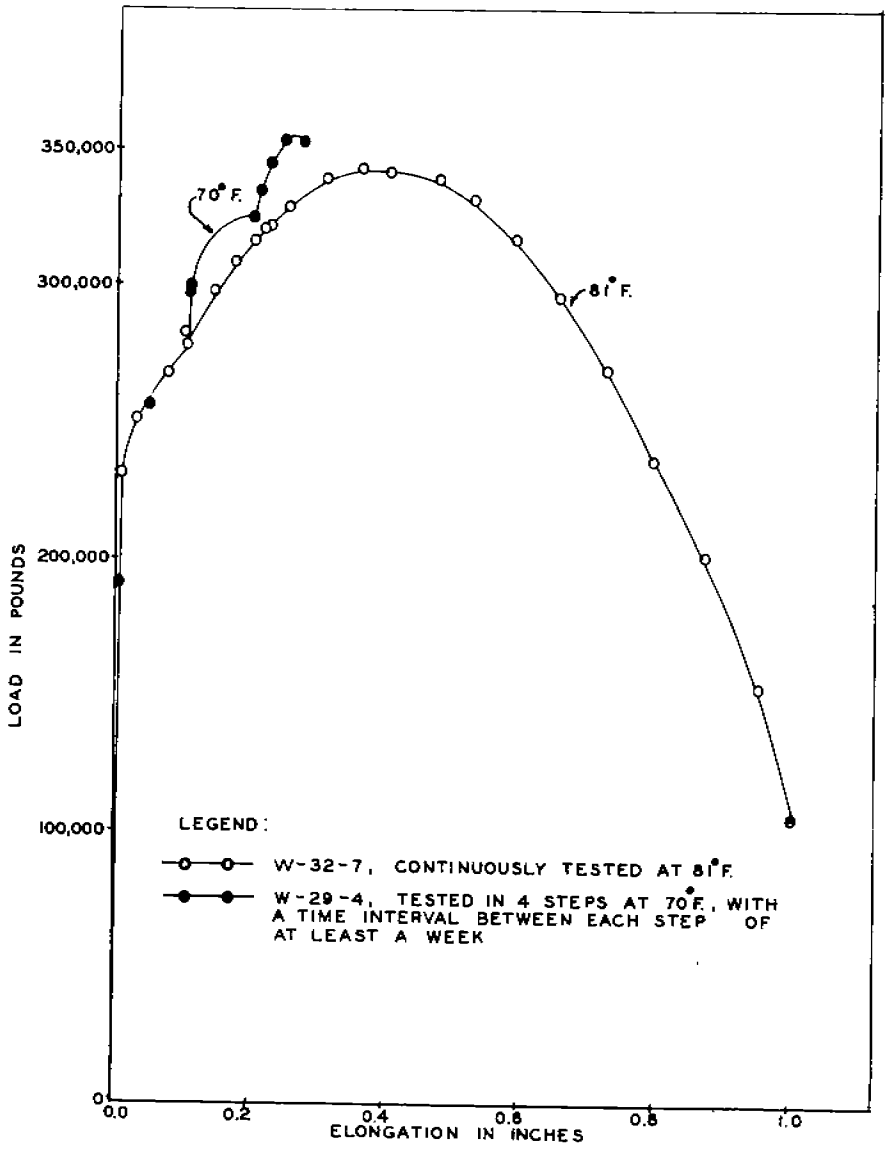

FIG. 21 EFFECT OF STRAIN AGING ON LOAD-DEFORMATION CURVE

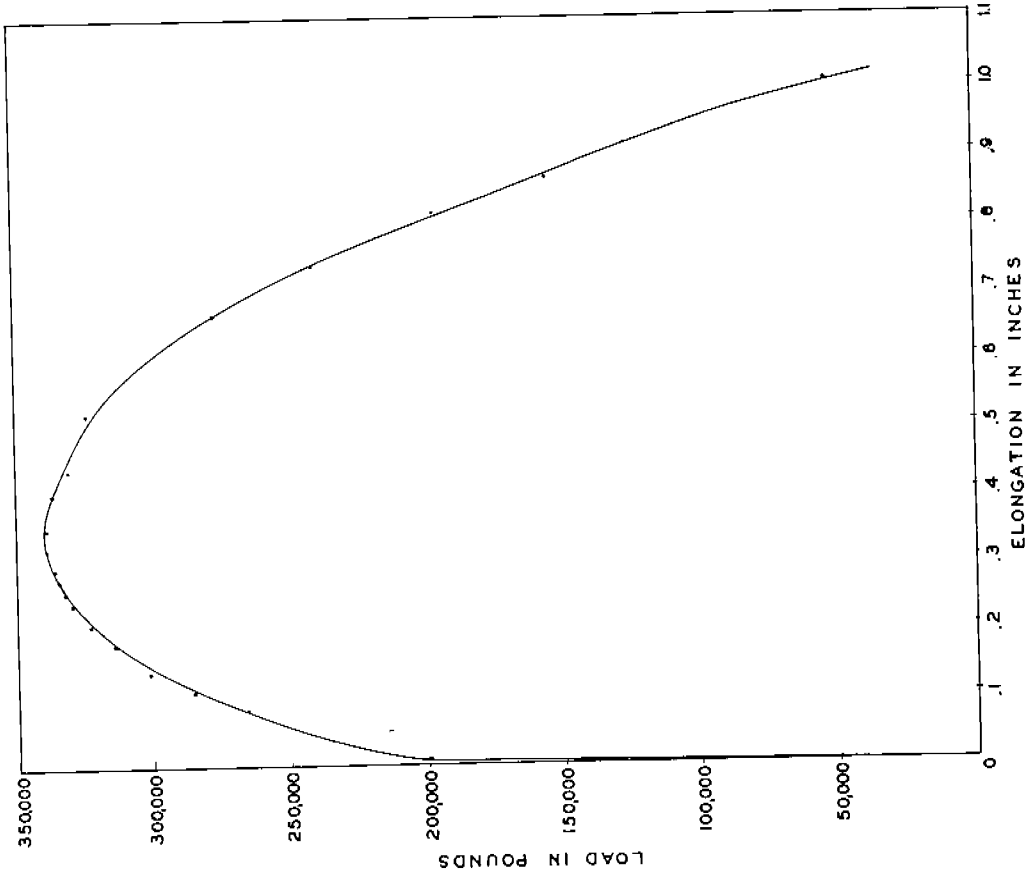

FIG. 23 CONTINUOUS LOAD – ELONGATION CURVE FOR W-29-4 AT 70°F.

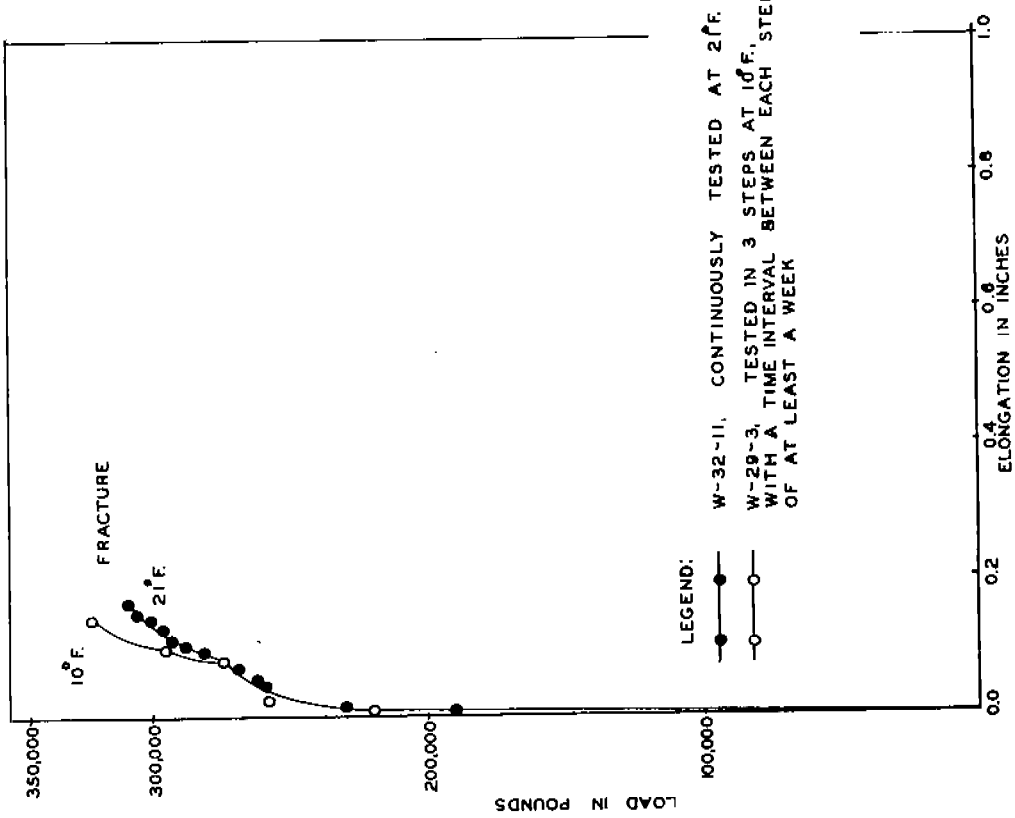

FIG. 22 EFFECT OF STRAIN AGING ON LOAD-DEFORMATION CURVE

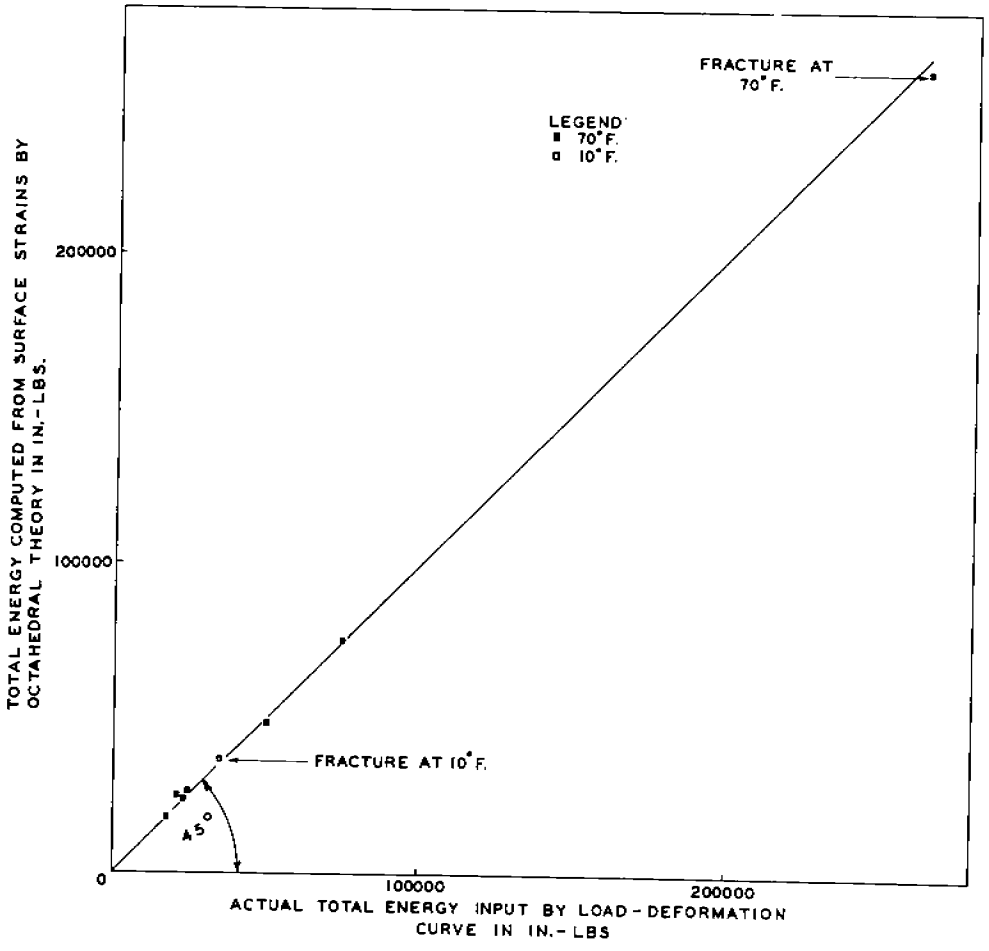

FIG. 24 COMPARISON OF TOTAL STRAIN ENERGY BASED ON SURFACE STRAINS AND OCTAHEDRAL THEORY AGAINST ACTUAL TOTAL ENERGY INPUT

SWARTHMORE COLLEGE
8-20-50

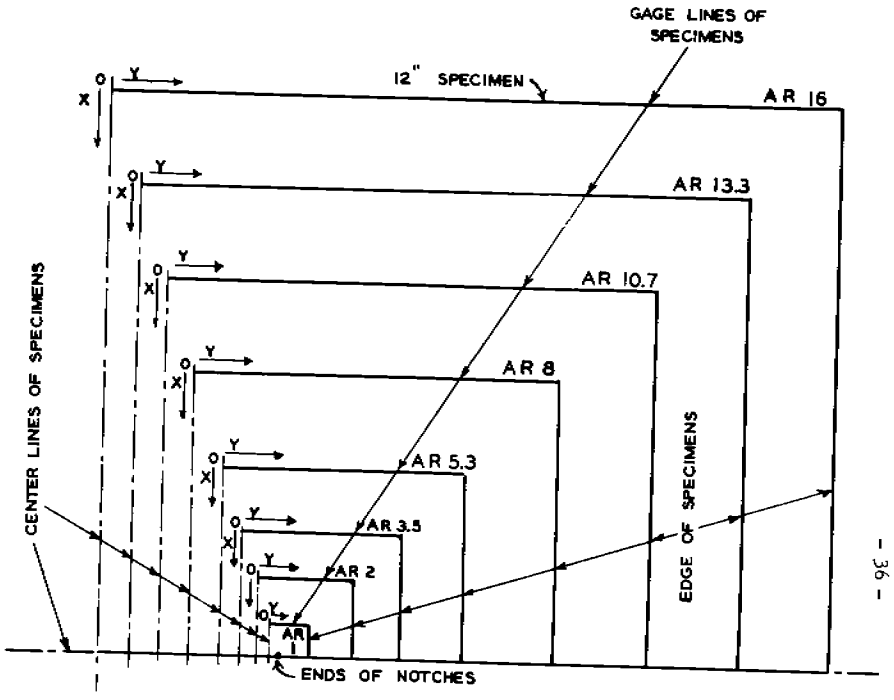

FIG. 25 QUARTER VIEW, SHOWING OUTLINES OF SPECIMEN WITH TWO-DIMENSIONAL SIMILARITY SUPERIMPOSED ON THE SURFACE OF A 12" SPECIMEN, WITH ALL NOTCH ENDS COINCIDING WITH EACH OTHER.

SWARTHMORE COLLEGE
1-13-50

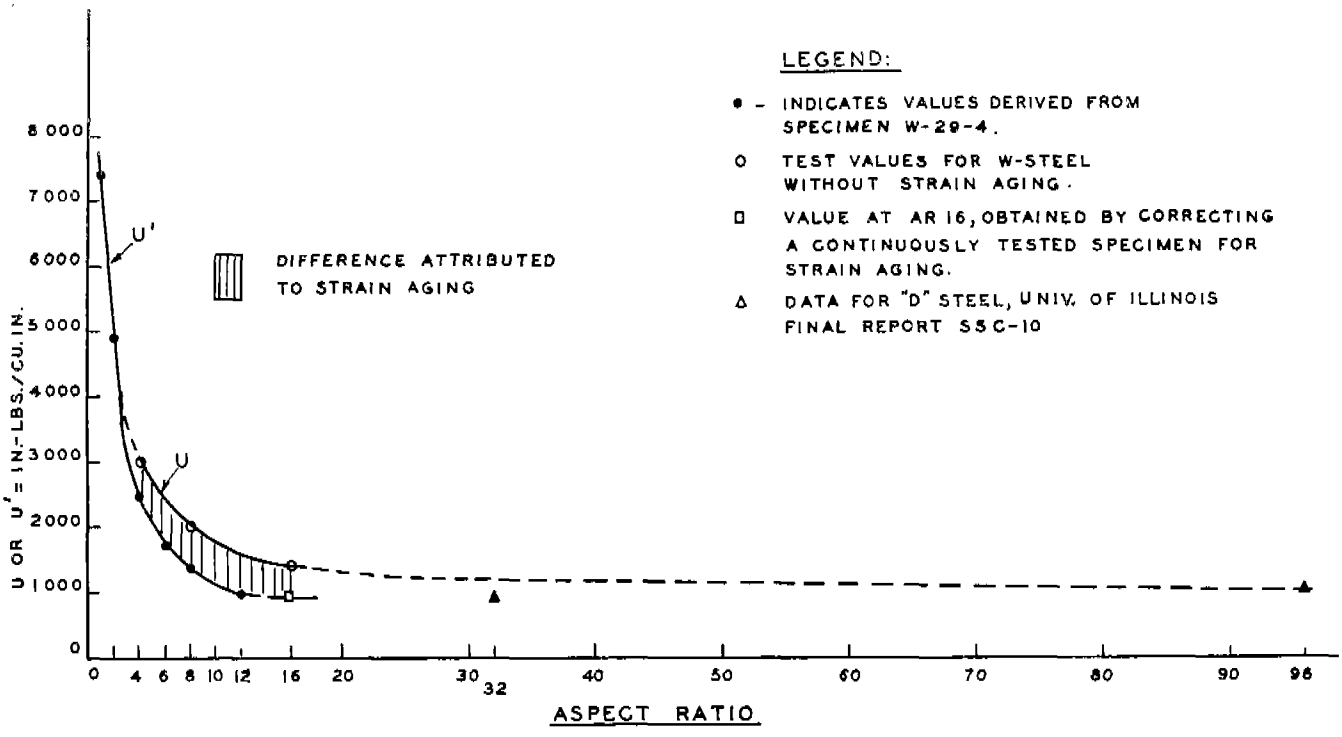

FIG. 26 CORRELATION BETWEEN THE UNIT STRAIN ENERGY DISTRIBUTION IN A 12"x 3/4" NOTCHED SPECIMEN AND THE AVERAGE UNIT ENERGY OF 3/4" THICK NOTCHED SPECIMENS, VARYING IN WIDTH.

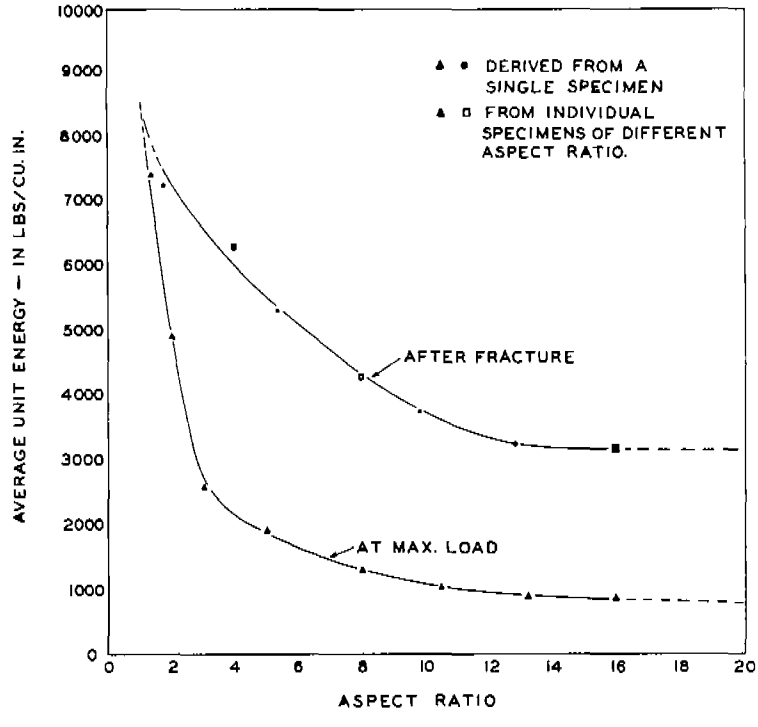

FIG. 27 CORRELATION (UPPER CURVE) BETWEEN THE UNIT STRAIN ENERGY DISTRIBUTION IN A FRACTURED 12"X3/4" NOTCHED SPECIMEN AND THE AVERAGE UNIT ENERGY OF FRACTURED 3/4" NOTCHED SPECIMEN VARYING IN WIDTH.